

UNSW
AUSTRALIA

SCHOOL OF ELECTRICAL ENGINEERING
AND TELECOMMUNICATIONS

Resource Allocation for IRS-Assisted Pinching Antenna Systems

by

Zipeng Ma

Thesis submitted as a requirement for the degree
Master of Engineering Science (Telecommunications)

Submitted: August 6, 2026

Supervisor: Prof Derrick Wing Kwan Ng
Co-supervisor: Dr Shaokang Hu

Abstract

The design of IRS and PAs together forms a fascinating network setup that can help make future 6G wireless connections more efficient and effective.In this case, the current research considers a downlink IRS-aided PA MISO system, wherein the use of a dielectric waveguide equipped with PAs is employed to improve near-field communication, whereas IRS serves as a medium for far-field communication owing to its reflective nature. This system has been modeled using spherical wave PA-user propagation, PA-BS feeding channel, and IRS assisted far-field channel.

Taking all these factors into consideration, an optimization problem for joint rate maximization is posed with respect to the transmit beamforming vectors of the base station, the IRS phase shifts, and the locations of the PAs while considering constraints on the transmit power, QoS, unit modulus, and PA mobility. However, this optimization problem is highly non-convex because of the inclusion of multi-user interference terms, the nonlinear nature of IRS phase shifts and PA location variables in the channel model, and the correlation between user rates. Therefore, this paper proposes the design of an alternating optimization method that consists of SOCP-based beamforming design, successive convex approximation-based IRS phase design, DC reformulation and successive convex approximation-based PA position design. Alternating optimization technique may be applied to solve the non-convex resource allocation problem. Simulation results show that the proposed IRS-assisted pinching antenna algorithm performs better than the existing ones in terms of sum rate performance with QoS constraints, transmit power constraint, IRS unit modulus, and PA mobility constraint.

Keywords— Intelligent Reflecting Surface (IRS), Dielectric Waveguide, Pinching Antenna (PA), Beamforming Optimization, Alternating Optimization, Spectral Efficiency.

Table of Contents

Abstract 1

List of Figures 4

List of Tables 5

Abbreviations 6

1 Introduction 9

1.1 Introduction . . . 9

2 Background 11

2.1 Background . . . 11

2.2 Related Work . . . 12

2.2.1 IRS-Assisted Communications and Joint Resource Allocation . . . 12

2.2.2 Near-Field, Far-Field, and Hybrid-Field Propagation . . . 13

2.2.3 Movable, Fluid, and Pinching Antennas . . . 14

2.2.4 Joint IRS–Pinching-Antenna Systems and Research Gap . . . 15

3 System Model 16

3.1 System Model . . . 16

4 Channel Model 19

4.1 Channel Model . . . 19

4.1.1 Direct BS-User Channels . . . 19

4.1.2 PA-Assisted Near-Field Channels . . . 19

4.1.3 IRS-Assisted Far-Field Channels . . . 21

4.2 Signal Model . . . 21

4.3 SINR and Rate Expressions . . . 22

5 Problem Formulation 23

5.1 Problem Formulation . . . 23

6 Solution of the Optimization Problem **24**
6.1 Problem Transformation 24
6.2 Beamforming Optimization 26
6.3 IRS Phase Optimization 27
6.4 PA Position Optimization 30
6.5 Overall AO Algorithm 32
6.6 Convergence Analysis 33
6.7 Complexity Analysis 33
6.8 Simulation Setup 35
6.9 Baseline Schemes 37
6.10 Numerical Results 38

7 Conclusion and Future Work **43**
7.1 Conclusion 43
7.2 Future Work 44

List of Figures

3.1 System model 16

6.1 Convergence performance of the AO algorithm. 38
6.2 IRS reflecting elements N_i on the achievable system sum rate. 38
6.3 Effect of the transmit power $P_{\max}$ on the system sum rate. 39
6.4 System sum rate under different total numbers of users K_{total}. 40
6.5 Influence of the amount of pinching antennas N_p on the achievable system sum rate. 40
6.6 System sum rate under different minimum QoS rate requirements $R_{\min}$. . . 41

List of Tables

6.1 Default Simulation Configuration 36

Abbreviations

6G	Sixth-Generation Wireless Networks
5G	Fifth-Generation Wireless Networks
IRS	Intelligent Reflecting Surface
RIS	Reconfigurable Intelligent Surface
RE	Reflecting Element (of an IRS)
PA	Pinching Antenna
BS	Base Station
MISO	Multiple-Input Single-Output
MIMO	Multiple-Input Multiple-Output
mmWave	Millimeter Wave
THz	Terahertz
IoT	Internet of Things
NOMA	Non-Orthogonal Multiple Access
LoS	Line-of-Sight
NLoS	Non-Line-of-Sight
NF	Near-Field
FF	Far-Field
AWGN	Additive White Gaussian Noise
CSI	Channel State Information
QoS	Quality of Service
SNR	Signal-to-Noise Ratio
SINR	Signal-to-Interference-plus-Noise Ratio
Rician K_R	Rician Fading Factor
R_{Rayleigh}	Rayleigh Distance
RF	Radio Frequency

Notation

Italic lower-case letters denote scalars, bold lower-case letters denote vectors, and bold upper-case letters denote matrices. The operators $(\cdot)^T$ and $(\cdot)^H$ represent the transpose and Hermitian transpose, respectively. The expectation operator is denoted by $\mathbb{E}\{\cdot\}$, and $\mathcal{CN}(\mu, \mathbf{R})$ denotes the circularly symmetric complex Gaussian distribution with mean μ and covariance $\mathbf{R}$.

The mathematical symbols we use in this report are listed below.

M	Number of BS antennas
K	Number of near-field users
J	Number of far-field users
$\mathcal{K}$	Set of near-field users
$\mathcal{J}$	Set of far-field users
$\mathcal{U}$	Set of all users
N_p	Number of pinching antennas (PAs)
N_i	Number of IRS reflecting elements
$\mathbf{w}_k$	Beamforming vector for user k
s_k	Transmit information symbol for user k
$P_{\max}$	Maximum BS transmit power
$\mathbf{x}$	BS transmit signal vector
n_k	AWGN noise at near-field user k
n_j	AWGN noise at far-field user j
$\mathbf{\Theta}$	IRS reflection (phase shift) matrix
θ_n	Phase shift of the n-th IRS element
β_n	Amplitude reflection coefficient of the n-th IRS element
$\boldsymbol{\psi}_n^{\mathrm{PA}}$	3D coordinate of the n-th PA
x_n^{PA}	Longitudinal position of PA along waveguide
d	Installation height of PAs
$\boldsymbol{\psi}_k^{\mathrm{near}}$	Coordinate of near-field user k
$\boldsymbol{\psi}_j^{\mathrm{far}}$	Coordinate of far-field user j
$\boldsymbol{\psi}_{\mathrm{I}}$	IRS coordinate
L_{area}	Side length of deployment area
L_{PA}	Length of PA waveguide
L_{th}	Near-/far-field distance threshold
$\mathbf{h}_{d,k}$	Direct BS–near-user channel
$\mathbf{h}_k^{\mathrm{PA}}$	Composite PA–near-user channel
$h_{k,n}^{\mathrm{PA-U_N}}$	PA–near-user channel via n-th PA
$\mathbf{g}_n^{\mathrm{PA}}$	BS–PA waveguide feeding channel
$\mathbf{h}_{r,j}$	IRS–far-user channel
$\mathbf{G}$	BS–IRS channel matrix
$\mathbf{H}_{\mathrm{PA-I}}$	PA–IRS near-field channel matrix
$d_{k,n}^{\mathrm{UPA}}$	Distance between PA n and near-user k
$d_{j,n}^{\mathrm{PA-U_F}}$	Distance between PA n and far-field user j
$d_{\mathrm{IN},k}$	IRS–near-user distance
$\mathrm{SINR}_{\mathrm{N},k}$	SINR of near-field user k
$\mathrm{SINR}_{\mathrm{F},j}$	SINR of far-field user j
$R_{N,k}$	Achievable rate for user k
$R_{F,j}$	Achievable rate for user j
$R_{\min}$	Minimum QoS rate requirement
λ	Wavelength of carrier signal
λ_g	Waveguide wavelength
η	PA coupling attenuation factor
α_D	Dielectric waveguide attenuation coefficient
β_n	Amplitude reflection coefficient of the n-th IRS element
K_R	Rician K-factor
β_0	Path-loss constant at 1 m
R_{Rayleigh}	Rayleigh distance $\frac{2D^2}{\lambda}$

Chapter 1

Introduction

1.1 Introduction

The emergence of 6G wireless communication networks will result in major innovations with respect to the speed, spectral efficiency, reliability, and energy sustainability of this technology [1,2]. To accomplish these aims, the latest research suggests that there should be a change of the environment of wireless communications from being passive to intelligent and controllable [3–7]. In terms of various approaches to enhancing the wireless communications environment, IRS (intelligent reflection system) [8] can be seen as one of the best solutions. Using the control of the phase shift of the near-passive reflector, the IRS changes the pattern of the electromagnetic wave.

At the same time, pinching antennas have recently been proposed to be used as an inexpensive and reconfigurable antenna structure that could be able to control the radiation point on the dielectric waveguide. The ability to configure the antenna would enable to attain near-field focusing ability and thus improve the spatial selectivity. This would be effective concerning the increased transmission efficiency and decreased interference level. However, although IRS and PAs have a lot of potential in improving the efficiency of wireless transmission, the current literature focuses on them separately without their complementary capabilities.

The utilization of IRS with pinching antennas can provide potential research opportunities in the field of intelligent wireless communications. In such a hybrid design of incorporating IRS into PA, both near-field focusing and far-field reflection of the signals can be utilized to realize efficient and flexible signal propagation control in intelligent wireless communications for users located in different areas. Challenges in modeling the channel of near-field and far-field jointly, joint optimization of IRS phase shifts and PA locations, and optimization algorithms development are faced in this scenario.

Given that challenges mentioned above exist, we will examine an IRS aided pinching antenna MISO communication system in this paper. In other words, the propagation

pattern of a spherical wave in the near-field region and of a plane wave in the far-field region can be achieved through the establishment of the uniform channel model. Then a joint optimization model is developed to enhance the communication rate.

Chapter 2

Background

2.1 Background

Some of the key aspects that will be used to develop the next generation of wireless technology (6G) are the requirements for very high data rates, very low latency, wide-area connections, and energy efficiency. While there have been some improvements in terms of enhancing the capabilities of mobile broadband as well as the massive internet of things using the technology of 5G, there are some issues associated with the technology of 5G, and these include energy efficiency, spectrum efficiency, and even coverage of complex environments. As such, there will be the need for a proper design architecture which will allow the provision of connectivity through the use of land based, air based, and space based systems and intelligent and immersive and ubiquitous communication service.

Terahertz communication, massive MIMO, dense cell deployment, and non-orthogonal multiple access have been viewed as some of the possible solutions. Although they have the capability to increase capacity and spectral efficiency, they pose several difficulties during implementation. For instance, the massive MIMO technology needs many radio frequency connections and the cost of channel estimation is relatively high, while dense cell deployment incurs high installation and operational costs. All this shows that there is a need for developing new design philosophies to gain notable performance improvements without complicating the hardware and power consumption.

In this context, IRS has emerged as an extremely promising approach for the development of 6G systems. The devices based on IRS can ensure optimization of the propagation environment through controlling the phase of passive reflection elements, which helps improve the necessary signal level, minimize interference, and extend coverage. Compared to conventional active amplifiers used for improving the signal, which utilize power amplifiers, IRS uses passive reflection, which provides benefits including energy efficiency, cost savings, and easy scalability. IRS is poised to become a driving factor in future wireless systems.

2.2 Related Work

This section reviews the research most relevant to the proposed intelligent reflecting surface (IRS)-assisted pinching-antenna system: (i) programmable propagation and joint active/passive beamforming, (ii) near-field and mixed-field channel models, (iii) position-reconfigurable antennas and dielectric-waveguide pinching antennas, and (iv) existing joint IRS–pinching-antenna designs. The discussion distinguishes the physical assumptions and optimization variables of each line of work rather than treating all reconfigurable wireless architectures as equivalent.

2.2.1 IRS-Assisted Communications and Joint Resource Allocation

IRS technology enables a transmitter to shape an indirect propagation path through controllable reflecting coefficients. The broader role of programmable propagation in 6G networks is surveyed in [9–12], while joint transmitter and reflection design was established for IRS-assisted wireless links in [13]. Such designs require a careful balance between channel enhancement, interference suppression, practical reflection constraints, and the availability of channel state information (CSI). Björnson and Sanguinetti [14] further demonstrated why power scaling and near-field effects must be considered when modeling large intelligent surfaces.

A series of studies coauthored by Ng developed robust and power-efficient formulations for these joint design problems. Robust and secure IRS-assisted communications were investigated in [15]; the subsequent green-communications formulation in [16] studied convergence and robust resource allocation. Self-sustainable IRS hardware and the associated multiuser sum-rate trade-offs were examined in [8]. Globally optimal resource allocation for discrete IRS phase shifts, including imperfect-CSI settings, was considered in [17]. In contrast to ideal continuously adjustable elements, such models recognise that finite-resolution reflection control constrains what can be achieved by passive beamforming. Weighted sum-rate optimization for multiple IRSs and full-duplex hardware impairments was treated in [18], illustrating the coupling between reflective paths and transmit-side interference.

Passive reflecting surfaces are not the only available architecture. Active IRSs use amplification and therefore require additional power and noise modeling [19]; active/passive hybrid configurations have likewise been investigated in [20]. Resource allocation for active IRS systems was studied in [21], which optimized beamforming in a wireless information-and-power-transfer setting. Related scalable IRS-assisted SWIPT formulations and nonlinear energy-harvesting constraints were addressed in [22, 23]. Although the service requirements differ from this thesis, these studies are useful methodological examples of

alternating optimization and coupled active/passive design under nonconvex constraints.

Realizable IRS control also depends on channel acquisition and hardware configuration. Codebook-based RIS solutions and their practical limitations were discussed in [24], whereas RIS-aided MIMO channel recovery using atomic-norm methods was investigated in [25]. Deep-residual learning for multiuser IRS channel estimation was studied in [26]. The effects of channel uncertainty, limited backhaul, and spatial correlation on IRS-enabled network beamforming were considered in [27,28]. Joint distributed precoding and RIS beamforming in cell-free massive MIMO systems were examined in [29], while data-driven optimization of RIS-aided cell-free systems was explored in [30, 31]. These works motivate an explicit treatment of CSI assumptions and hardware limitations; however, they do not jointly model the movement of radiating points along a dielectric waveguide and the phases of an external IRS, as required in the present system.

2.2.2 Near-Field, Far-Field, and Hybrid-Field Propagation

The electromagnetic propagation regime is especially important for spatially reconfigurable transmitters. When the distance between an antenna aperture and a receiver is not sufficiently large relative to the aperture size and wavelength, spherical wavefronts and spatial focusing effects cannot be captured adequately by a plane-wave approximation [32]. Near- and far-field behavior also affects RIS-aided localization and beamforming [33, 34].

An integrated treatment of both propagation regimes was developed for holographic MIMO from a wavenumber-domain viewpoint in [35]. The effective spatial degrees of freedom of near-field extremely large-scale MIMO systems were characterized in [36]. For RIS-assisted MIMO, the piecewise near-field model in [37] offers a useful alternative to treating an extended array with a single global far-field approximation. Mixed near- and far-field RIS-assisted resource allocation with directional antennas was addressed in [38]. Further, hybrid near-/far-field six-dimensional movable-antenna design was explored in [39]; that architecture changes the antenna configuration itself rather than relying only on passive reflecting coefficients.

Near-field channel estimation and beam focusing form another relevant research direction. Sensing-enhanced estimation was investigated in [40]; other solutions used generative priors or spatial-domain channel extrapolation [41,42]. Near-field arrays were also used to infer user activity, channels, and locations in [43]. Energy-efficient hybrid beam focusing and robust spherical-wavefront beamforming were examined for near-field integrated sensing and communication in [44,45]. Related STAR-RIS-assisted hybrid-field beamforming was explored in [46]. These studies provide useful modeling and optimization precedents, but their sensing-oriented metrics or array architectures should not be conflated with the rate-maximization problem studied here.

For the present thesis, near-field pinching-antenna–user links are represented using

position-dependent distances and spherical phases, whereas the IRS-aided far-field links are modeled under the assumed plane-wave regime. Such a mixed-field model is appropriate only when the relevant link distances and apertures satisfy the assumptions of each approximation. This distinction is critical because the positions of the pinching antennas influence both propagation losses and phases, not merely the steering direction of a conventional fixed array.

2.2.3 Movable, Fluid, and Pinching Antennas

A complementary line of research improves wireless links by changing the position or configuration of the radiating antennas rather than controlling a reflection surface alone. Globally optimal discrete positioning and beamforming for movable-antenna multiuser links were studied in [47]. Two-timescale sum-rate optimization for movable antennas was examined in [48], while distributed position adaptation and learning-based coordination appear in [49]. Movable antennas have also been considered for relay optimization in [50]. These studies show that spatial degrees of freedom can be optimized alongside transmit precoders, although their antenna actuation mechanisms differ from the guided-wave pinching structure.

Fluid antennas provide a related form of reconfigurability; their operating principles and applications are surveyed in [51]. Fluid-antenna position control has been investigated for multiuser MIMO integrated sensing and communications [52]. Systems that combine fluid or movable antennas with reflective surfaces have also been studied using two-timescale analysis, over-the-air computation, and beyond-diagonal RIS architectures [53–55]. These papers demonstrate the potential benefits of controlling both antenna configurations and propagation paths. Nevertheless, a fluid antenna's selectable ports, a freely movable radiator, and a pinching antenna attached to a dielectric waveguide have distinct movement, feeding, attenuation, and phase constraints.

Pinching-antenna systems (PASSs) specifically create reconfigurable radiation points on one or more dielectric waveguides. Their performance depends on the selected pinching locations, guided-wave phase accumulation, waveguide attenuation, and wireless propagation from each radiating point. Their outage and average-rate behavior was studied in [56]; multiuser capacity characteristics were examined in [57]. The principles and deployment options of generalized PASSs were reviewed in [58], while resource allocation methods and open challenges were surveyed in [59]. PA position and power design for simultaneous wireless information and power transfer was investigated in [60, 61], showing how location optimization couples to conventional precoding and power control.

Hu et al. [62] considered sum-rate maximization for NOMA with multiple di-electric waveguides, and Zhao et al. [63] studied resource allocation for multi-waveguide

broadcast networks. Robust and secure blockage-aware PA communications were developed in [64], extending the basic positioning problem to propagation blockage and uncertainty. Waveguide mode selection for pinching-antenna-assisted integrated sensing and communications was considered in [4]. These contributions directly motivate the use of physically meaningful PA locations and waveguide constraints, but the network architectures and performance criteria are not identical to the combined IRS-assisted multiuser system in this thesis.

2.2.4 Joint IRS–Pinching-Antenna Systems and Research Gap

An IRS and a PASS offer two different, potentially complementary mechanisms. The PASS repositions radiation points along a feeding waveguide, whereas the IRS redirects incident fields by adjusting its reflecting coefficients. Joint design therefore couples the base station (BS) transmit precoder, waveguide-constrained PA positions, and IRS reflection phases through the users' received signals. Existing work has begun to address this coupling directly. In [65], reinforcement learning was investigated for beamforming in RIS-assisted pinching-antenna systems. He et al. [66] considered graph-neural-network-based optimization of PA positions, RIS phases, and beamforming in an IRS-assisted downlink setting, with an extension to multiple BSs and RISs in [67]. These studies preclude a broad claim that joint IRS–PASS optimization has never been studied.

The contribution pursued in this thesis is therefore more specific: a joint resource-allocation formulation for a BS-driven IRS-assisted PASS serving users under the stated mixed near-/far-field channel assumptions, with a conventional optimization-based procedure for adjusting BS transmit beamformers, IRS reflection phases, and waveguide-constrained pinching locations. The combination of position-dependent near-field propagation, IRS-assisted links, quality-of-service (QoS) requirements, and coupled nonconvex design variables motivates a structured alternating-optimization approach. Compared with learning-based IRS–PASS work, this approach exposes the model assumptions and the subproblem approximations explicitly; it does not, by itself, establish global optimality.

The main technical questions addressed by the thesis are thus (i) whether the adopted channel and waveguide models capture the relevant phase and attenuation variations, (ii) how the three sets of design variables influence users' achievable rates and interference, and (iii) how feasible updates of the BS beamformers, IRS phases, and PA positions can be obtained efficiently. The contribution should be judged against these specific modeling and algorithmic choices rather than against an unsupported claim that all prior IRS-assisted PA studies use learning or omit joint design.

Chapter 3

System Model

3.1 System Model

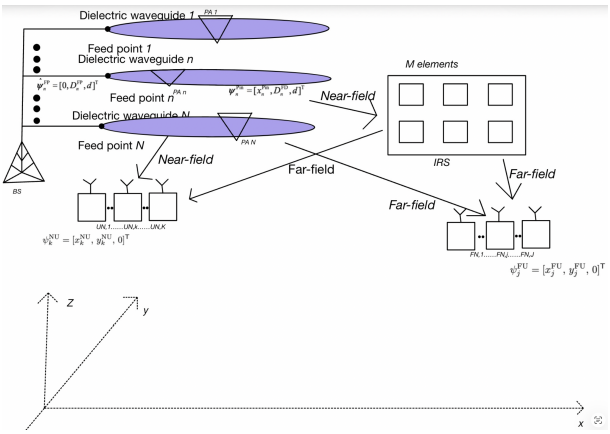

Figure 3.1: System model

Figure 3.1 introduces the downlink multiple-input single-output (MISO) communication model which is consisted of a combination of a pinching antenna (PA) array and intelligent reflecting surface (IRS) to improve the near-field and far-field wireless communications.

The system includes one base station (BS), K near-field users, and J far-field users that are all randomly deployed in a square area of size $L_{\text{area}} \times L_{\text{area}}$. To support adaptive transmission, the base station is connected to N_p low-loss dielectric waveguides, with each waveguide carrying one movable PA. Unlike conventional fixed antenna arrays, each PA can slide continuously along its corresponding waveguide, enabling flexible adjustment of its radiation position according to the communication environment.

Since this work focuses on communication system optimization rather than electromagnetic waveguide implementation, the physical dielectric material is not explicitly specified. Instead, wave propagation inside the dielectric waveguide is characterized by two effective parameters: the effective refractive index n_{eff} and the propagation attenuation coefficient α_D. These parameters capture the dominant propagation characteristics required

for communication system design while avoiding unnecessary hardware-level modeling complexity.

The position of the n-th PA is represented by

$$\boldsymbol{\psi}_n^{\mathrm{PA}} = [x_n^{\mathrm{PA}},\, D^{\mathrm{FP}},\, d]^T,$$

where x_n^{PA} denotes the longitudinal position along the waveguide, D^{FP} is the fixed lateral offset, and d represents the installation height.

Similarly, the coordinates of the k-th near-field user and the j-th far-field user are respectively expressed as

$$\boldsymbol{\psi}_k^{\mathrm{near}} = [x_k^{\mathrm{near}},\, y_k^{\mathrm{near}},\, 0]^T,$$

and

$$\boldsymbol{\psi}_j^{\mathrm{far}} = [x_j^{\mathrm{far}},\, y_j^{\mathrm{far}},\, 0]^T.$$

The IRS is installed at a fixed location

$$\boldsymbol{\psi}_{\mathrm{I}} = [x_I, y_I, z_I]^T,$$

where it passively manipulates the wireless propagation environment by creating additional reflected transmission paths to improve the overall channel quality.

The waveguide structure of this design is primarily meant for serving users within the near-field regime, since spherical wave propagation will allow for better focusing and more efficient transmission. The boundary between near and far-field regions is given by Rayleigh Distance.

$$R_{\mathrm{Rayleigh}} = \frac{2D^2}{\lambda}, \tag{3.1}$$

where D denotes the aperture size and λ is the carrier wavelength.

As the communication distance increases, the coupling gain provided by the dielectric waveguide gradually decreases. In particular, when the separation distance between the user and its respective waveguide is greater than the threshold L that is defined as

$$\|\boldsymbol{\psi}_k^{\mathrm{near}} - \boldsymbol{\psi}_n^{\mathrm{PA}}\| > L,$$

the coupling attenuation becomes significant. Such users are therefore regarded as far-field users in the proposed system.

To provide reliable communication for these users, an IRS containing N_i passive reflectors can be used to create further transmission routes through reflection, thus improving the gain of the overall channel.

In this entire thesis, it should be noted that all communication channels would have the characteristics of quasi-static flat fading communication channel where the channel

gains do not change within a coherence time interval.

Chapter 4

Channel Model

4.1 Channel Model

In this paper, we study a downlink IRS-based PA-assisted pinching antenna system in which a base station with M antennas transmits to two sets of users with a single antenna. We refer to the group of near-field users as $\mathcal{K}$ and the far-field users as $\mathcal{J}$. The BS has the number of PAs (N_p) attached through a dielectric waveguide, and an IRS with (N_i) reflective elements is utilized for the far-field transmission.

4.1.1 Direct BS-User Channels

The direct BS-to-near-field-user channel and BS-to-far-field-user channel are denoted by

$$\mathbf{h}_{d,k} \in \mathbb{C}^{M\times 1}, \quad k \in \mathcal{K}, \tag{4.1}$$

and

$$\mathbf{h}_{d,j} \in \mathbb{C}^{M\times 1}, \quad j \in \mathcal{J}, \tag{4.2}$$

respectively. A standard path-loss model can be written as

$$\mathbf{h}_{d,k} = \sqrt{\beta_0 d_k^{-\alpha}}\, \tilde{\mathbf{h}}_{d,k}, \quad \mathbf{h}_{d,j} = \sqrt{\beta_0 d_j^{-\alpha}}\, \tilde{\mathbf{h}}_{d,j}, \tag{4.3}$$

where β_0 is the reference channel gain, α is the path-loss exponent, and $\tilde{\mathbf{h}}_{d,k}$ and $\tilde{\mathbf{h}}_{d,j}$ denote small-scale fading vectors.

4.1.2 PA-Assisted Near-Field Channels

For the PA-assisted near-field link, two components must be distinguished: the BS-to-PA feeding channel and the PA-to-user spherical-wave channel. Let $\mathbf{g}_n^{PA} \in \mathbb{C}^{M\times 1}$ denote the BS-to-n-th-PA feeding/channel vector. If the PA is fed through a dielectric waveguide

rather than a wireless BS-to-PA link, $\mathbf{g}_n^{PA}$ should be interpreted as the effective waveguide feeding response seen from the BS beamforming vector.

The scalar channel from PA n to near-field user k is modeled as

$$a_{k,n}^{\mathrm{PA}}(x_n^{\mathrm{PA}}) = \frac{\sqrt{\eta}}{d_{k,n}} \exp\left(-j\frac{2\pi}{\lambda}d_{k,n} - j\frac{2\pi}{\lambda_g}x_n^{\mathrm{PA}} - \alpha_D x_n^{\mathrm{PA}}\right), \tag{4.4}$$

where $d_{k,n} = \|\boldsymbol{\psi}_k^{\mathrm{near}} - \boldsymbol{\psi}_n^{\mathrm{PA}}\|$ is the distance between PA n and near-field user k, λ is the carrier wavelength, The carrier wavelength is

$$\lambda = \frac{c}{f_c},$$

where f_c denotes the carrier frequency.

The guided wavelength is

$$\lambda_g = \frac{\lambda}{n_{\mathrm{eff}}},$$

where n_{eff} is the effective refractive index of the dielectric waveguide. and α_D is the dielectric attenuation coefficient.

The above expression represents the physical propagation model for the PA assisted communication link, which includes free space propagation, guided wave propagation, and dielectric loss. Since this thesis focuses on system-level resource allocation rather than electromagnetic waveguide design, the numerical simulations adopt a normalized narrowband channel model. In particular, the PA-assisted channel magnitude is represented by

$$\left|a_{k,n}^{\mathrm{PA}}\right| = \sqrt{\beta_0 d_{k,n}^{-\alpha}}, \tag{4.5}$$

where β_0 is the reference channel gain and α is the path-loss exponent. Therefore, the carrier-dependent phase, the guided-wave phase, and the dielectric attenuation are not explicitly evaluated in the current simulation implementation.

The PA-assisted effective channel from the BS antenna array to near-field user k is then

$$\mathbf{h}_{\mathrm{PA},k}^H = \sum_{n=1}^{N_p} a_{k,n}^{\mathrm{PA}}(x_n^{\mathrm{PA}})\mathbf{g}_n^H. \tag{4.6}$$

This definition gives $\mathbf{h}_{\mathrm{PA},k} \in \mathbb{C}^{M\times 1}$, so it can be added consistently to the direct BS-user channel.

4.1.3 IRS-Assisted Far-Field Channels

Thia channel is denoted by $\mathbf{G} \in \mathbb{C}^{N_i \times M}$ and is modeled as a Rician fading channel,

$$\mathbf{G} = \sqrt{\frac{K_R}{K_R+1}}\mathbf{G}^{\text{LoS}} + \sqrt{\frac{1}{K_R+1}}\mathbf{G}^{\text{NLoS}}, \tag{4.7}$$

where K_R is the Rician factor. The IRS-to-far-field-user channel is $\mathbf{h}_{r,j} \in \mathbb{C}^{N_i \times 1}$.

The IRS reflection matrix is

$$\mathbf{\Theta} = \text{diag}(v_1, \ldots, v_{N_i}), \mathbf{v} = [v_1, \cdots, v_{N_i}]^T \quad v_n = e^{j\theta_n}, \quad |v_n| = 1. \tag{4.8}$$

A lossless passive IRS model is assumed throughout this thesis. Accordingly, the amplitude reflection coefficient of each IRS element is fixed as

$$\beta_n = 1, \quad n = 1, \ldots, N_i, \tag{4.9}$$

and only the reflection phases $\{\theta_n\}$ are optimized.

Due to severe path loss, the PA-to-far-user and IRS-to-near-user links are neglected in this report. If these links are non-negligible in a later simulation setup, the SINR expressions should be extended accordingly.

4.2 Signal Model

The BS transmits independent symbols to all near-field and far-field users:

$$\mathbf{x} = \sum_{k \in \mathcal{K}} \mathbf{w}_k s_k + \sum_{j \in \mathcal{J}} \mathbf{w}_j s_j, \tag{4.10}$$

where $\mathbf{w}_k, \mathbf{w}_j \in \mathbb{C}^{M \times 1}$ are the beamforming vectors and $\mathbb{E}[|s_k|^2] = \mathbb{E}[|s_j|^2] = 1$. The transmit-power constraint is

$$\sum_{k \in \mathcal{K}} \|\mathbf{w}_k\|^2 + \sum_{j \in \mathcal{J}} \|\mathbf{w}_j\|^2 \leq P_{\max}. \tag{4.11}$$

For near-field user k, the effective channel is

$$\mathbf{h}_{N,k}^H = \mathbf{h}_{d,k}^H + \mathbf{h}_{\text{PA},k}^H. \tag{4.12}$$

The received signal is

$$y_k = \mathbf{h}_{N,k}^H \mathbf{x} + n_k, \quad n_k \sim \mathcal{CN}(0, \sigma_k^2). \tag{4.13}$$

For far-field user j, the effective channel is

$$\mathbf{h}_{F,j}^H = \mathbf{h}_{d,j}^H + \mathbf{h}_{r,j}^H \boldsymbol{\Theta} \mathbf{G}. \tag{4.14}$$

The received signal is

$$y_j = \mathbf{h}_{F,j}^H \mathbf{x} + n_j, \quad n_j \sim \mathcal{CN}(0, \sigma_j^2). \tag{4.15}$$

4.3 SINR and Rate Expressions

The SINR of near-field user k is

$$\mathrm{SINR}_{N,k} = \frac{|\mathbf{h}_{N,k}^H \mathbf{w}_k|^2}{\sum_{i \in \mathcal{K}, i \neq k} |\mathbf{h}_{N,k}^H \mathbf{w}_i|^2 + \sum_{j \in \mathcal{J}} |\mathbf{h}_{N,k}^H \mathbf{w}_j|^2 + \sigma_k^2}. \tag{4.16}$$

The SINR of far-field user j is

$$\mathrm{SINR}_{F,j} = \frac{|\mathbf{h}_{F,j}^H \mathbf{w}_j|^2}{\sum_{m \in \mathcal{J}, m \neq j} |\mathbf{h}_{F,j}^H \mathbf{w}_m|^2 + \sum_{k \in \mathcal{K}} |\mathbf{h}_{F,j}^H \mathbf{w}_k|^2 + \sigma_j^2}. \tag{4.17}$$

The achievable rates are

$$R_{N,k} = \log_2(1 + \mathrm{SINR}_{N,k}), \quad k \in \mathcal{K}, \tag{4.18}$$

and

$$R_{F,j} = \log_2(1 + \mathrm{SINR}_{F,j}), \quad j \in \mathcal{J}. \tag{4.19}$$

Accordingly, the system sum rate is expressed as

$$R_{\mathrm{sum}} = \sum_{k \in \mathcal{K}} R_{N,k} + \sum_{j \in \mathcal{J}} R_{F,j}. \tag{4.20}$$

Chapter 5

Problem Formulation

5.1 Problem Formulation

The problem statement will be based on the channel model and signal model presented in previous sections such that the objective function is to optimize the beamforming vectors of the BSs, IRS reflectivities, and the positions of PAs in order to maximize the sum rate of the entire system.

$$\mathbf{P1}: \max_{\{\mathbf{w}_k\},\{\mathbf{w}_j\},\boldsymbol{\Theta},\{x_n^{\mathrm{PA}}\}} \quad \sum_{k\in\mathcal{K}} R_{N,k} + \sum_{j\in\mathcal{J}} R_{F,j} \tag{5.1a}$$

$$\text{s.t.} \quad \mathbf{C1:}\ R_{N,k} \geq R_{\min}^{N}, \quad \forall k \in \mathcal{K}, \tag{5.1b}$$

$$\mathbf{C2:}\ R_{F,j} \geq R_{\min}^{F}, \quad \forall j \in \mathcal{J}, \tag{5.1c}$$

$$\mathbf{C3:}\ \sum_{k\in\mathcal{K}} \|\mathbf{w}_k\|^2 + \sum_{j\in\mathcal{J}} \|\mathbf{w}_j\|^2 \leq P_{\max}, \tag{5.1d}$$

$$\mathbf{C4:}\ |v_n| = 1, \quad n = 1,\ldots,N_i, \tag{5.1e}$$

$$\mathbf{C5:}\ 0 \leq x_n^{\mathrm{PA}} \leq L_{\mathrm{PA}}, \quad n = 1,\ldots,N_p. \tag{5.1f}$$

In problem **P1**, constraints C1 and C2 ensure that the minimum data rate achievable by near-field users and far-field users is assured. The constraint C3 limits the available total transmit power at the BS. The constraint C4 ensures that the constant modulus condition is fulfilled for the passive IRS. The constraint C5 ensures that the movable PA operates in its available movement region.

Although the mathematical formulation appears compact, problem **P1** is inherently non-convex. The biggest issue lies in the strong dependence of the beamforming vector, phase of the IRS, and the PA locations in both the objective and the constraint functions. The problem cannot thus be solved using direct optimization methods since it is infeasible to compute the global optimum point for such a problem. To solve this problem effectively, the next chapter proposes the application of Alternating Optimization (AO).

Chapter 6

Solution of the Optimization Problem

6.1 Problem Transformation

Chapter 5 formulated the resource-allocation task for the considered IRS-assisted pinching-antenna (PA) communication system. The objective is to maximize the achievable system sum rate through the joint optimization of the BS beamforming vectors $\{\mathbf{w}_k\}_{k\in\mathcal{K}}$ and $\{\mathbf{w}_j\}_{j\in\mathcal{J}}$, the IRS reflection vector $\mathbf{v} = [v_1, \ldots, v_{N_i}]^T$, together with the PA locations $\{x_n^{\mathrm{PA}}\}_{n=1}^{N_p}$.

However, solving the problem directly is quite challenging owing to the extremely non-convex nature of the problem. The problem of non-convexity can be attributed to the following factors. Firstly, the optimization variables are joint coupled in the SINR functions. Secondly, there is a need for the reflection coefficients of the IRS to satisfy the constant modulus constraint. Finally, the location of PAs is part of the near-field spherical wave channel model.

The description of constraints is provided below. The first two constraints C1 and C2 guarantee the satisfaction of the minimum QoS requirements of the near-field and far-field users, respectively. Constraint C3 guarantees the finiteness of the total available transmit power of the BS. Constraint C4 guarantees the unit-modulus condition of the IRS, while constraint C5 guarantees the range of each movable PA in the corresponding dielectric waveguide.

To facilitate the following derivation, define the unified user set

$$\mathcal{U} = \mathcal{K} \cup \mathcal{J}. \tag{6.1}$$

For user $u \in \mathcal{U}$, $\mathbf{h}_u$ and $\mathbf{w}_u$ denote the effective channel and beamforming vector, respectively. In particular, $\mathbf{h}_u = \mathbf{h}_{N,k}$ and $\mathbf{w}_u = \mathbf{w}_k$ for a near-field user $u = k \in \mathcal{K}$, while $\mathbf{h}_u = \mathbf{h}_{F,j}$ and $\mathbf{w}_u = \mathbf{w}_j$ for a far-field user $u = j \in \mathcal{J}$.

We introduce auxiliary SINR variables $\{\gamma_{N,k}\}_{k\in\mathcal{K}}$ and $\{\gamma_{F,j}\}_{j\in\mathcal{J}}$. Since

$$R_{N,k} = \log_2(1+\mathrm{SINR}_{N,k}), \quad R_{F,j} = \log_2(1+\mathrm{SINR}_{F,j}), \tag{6.2}$$

the QoS constraints C1 and C2 can be equivalently transformed into SINR lower-bound constraints. Therefore, the original sum-rate maximization problem can be rewritten as

$$\begin{aligned}
\mathbf{P2}: \quad \max_{\{\mathbf{w}_u\},\mathbf{v},\{x_n^{\mathrm{PA}}\},\boldsymbol{\gamma}} \quad & \sum_{k\in\mathcal{K}} \log_2(1+\gamma_{N,k}) + \sum_{j\in\mathcal{J}} \log_2(1+\gamma_{F,j}) && \text{(6.3a)}\\
\text{s.t.} \quad \widetilde{\mathrm{C1}}: \quad & \mathrm{SINR}_{N,k} \geq \gamma_{N,k} \geq 2^{R_{\min}^N} - 1, \quad \forall k \in \mathcal{K}, && \text{(6.3b)}\\
\widetilde{\mathrm{C2}}: \quad & \mathrm{SINR}_{F,j} \geq \gamma_{F,j} \geq 2^{R_{\min}^F} - 1, \quad \forall j \in \mathcal{J}, && \text{(6.3c)}\\
\widetilde{\mathrm{C3}}: \quad & \sum_{u\in\mathcal{U}} \|\mathbf{w}_u\|_2^2 \leq P_{\max}, && \text{(6.3d)}\\
\widetilde{\mathrm{C4}}: \quad & |v_n| = 1, \quad n = 1,\ldots,N_i, && \text{(6.3e)}\\
\widetilde{\mathrm{C5}}: \quad & 0 \leq x_n^{\mathrm{PA}} \leq L, \quad n = 1,\ldots,N_p. && \text{(6.3f)}
\end{aligned}$$

In **P2**, constraints $\widetilde{\mathrm{C1}}$ and $\widetilde{\mathrm{C2}}$ are obtained from the QoS constraints C1 and C2, respectively. Constraint $\widetilde{\mathrm{C3}}$ corresponds to the transmit-power constraint C3, while constraints $\widetilde{\mathrm{C4}}$ and $\widetilde{\mathrm{C5}}$ inherit the IRS unit-modulus constraint C4 and PA movement constraint C5, respectively.

Constraint $\widetilde{\mathrm{C1}}$ is obtained from the SINR expression of near-field user k and can be expanded as

$$|\mathbf{h}_{N,k}^H \mathbf{w}_k|^2 \geq \gamma_{N,k} \left(\sum_{i\in\mathcal{K}, i\neq k} |\mathbf{h}_{N,k}^H \mathbf{w}_i|^2 + \sum_{j\in\mathcal{J}} |\mathbf{h}_{N,k}^H \mathbf{w}_j|^2 + \sigma_k^2 \right). \tag{6.4}$$

Similarly, constraint $\widetilde{\mathrm{C2}}$ for far-field user j becomes

$$|\mathbf{h}_{F,j}^H \mathbf{w}_j|^2 \geq \gamma_{F,j} \left(\sum_{m\in\mathcal{J}, m\neq j} |\mathbf{h}_{F,j}^H \mathbf{w}_m|^2 + \sum_{k\in\mathcal{K}} |\mathbf{h}_{F,j}^H \mathbf{w}_k|^2 + \sigma_j^2 \right). \tag{6.5}$$

Equations (6.4) and (6.5) show that the SINR variables are multiplied by interference terms. In addition, $\mathbf{h}_{F,j}$ depends on the IRS reflection vector $\mathbf{v}$, and $\mathbf{h}_{N,k}$ depends on the PA positions $\{x_n^{\mathrm{PA}}\}$. Hence, **P2** remains non-convex.To find the suboptimal solution, we use an AO scheme in which we alternate the updating of the beamforming vectors, IRS phase shifts, and PA locations. Due to the coupling nature of the optimization variables in both the cost function and the constraints, the problem **P2** cannot be solved efficiently.

6.2 Beamforming Optimization

For given IRS reflection vector $\mathbf{v}$ and PA positions $\{x_n^{\mathrm{PA}}\}$, all effective channels are fixed. The remaining beamforming subproblem is still non-convex if the SINR targets are optimized jointly with the beamforming vectors. Therefore, following the standard SOCP reformulation for multi-user MISO beamforming, we fix the SINR targets during each beamforming update. Let $\bar{\gamma}_u$ denote the target SINR of user $u \in \mathcal{U}$ at the current AO iteration. The beamforming subproblem is written by preserving the original transmit-power constraint C3 and replacing the rate constraints with fixed SINR targets:

$$\mathbf{P3}: \quad \min_{\{\mathbf{w}_u\}_{u\in\mathcal{U}}} \quad \sum_{u\in\mathcal{U}} \|\mathbf{w}_u\|_2^2 \tag{6.6a}$$

$$\text{s.t.} \quad \text{B1}: \quad \mathrm{SINR}_u \geq \bar{\gamma}_u, \quad \forall u \in \mathcal{U}, \tag{6.6b}$$

$$\text{B2}: \quad \sum_{u\in\mathcal{U}} \|\mathbf{w}_u\|_2^2 \leq P_{\max}. \tag{6.6c}$$

Problem **P3** is obtained from the transformed QoS constraints $\widetilde{\text{C1}}$ and $\widetilde{\text{C2}}$ in **P2**. Even with fixed SINR targets, constraint B1 is still non-convex in its original fractional form because the desired beamforming vector and the interfering beamforming vectors are coupled in the SINR expression. To obtain a tractable convex subset, the SINR constraint is equivalently transformed into an SOC constraint as follows. Constraint B1 can be expressed as

$$\frac{|\mathbf{h}_u^H \mathbf{w}_u|^2}{\sum_{\ell\in\mathcal{U},\ell\neq u} |\mathbf{h}_u^H \mathbf{w}_\ell|^2 + \sigma_u^2} \geq \bar{\gamma}_u, \quad \forall u \in \mathcal{U}. \tag{6.7}$$

By cross multiplication, (6.7) becomes

$$|\mathbf{h}_u^H \mathbf{w}_u|^2 \geq \bar{\gamma}_u \left(\sum_{\ell\in\mathcal{U},\ell\neq u} |\mathbf{h}_u^H \mathbf{w}_\ell|^2 + \sigma_u^2 \right). \tag{6.8}$$

Taking the square root on both sides of (6.8), which preserves the inequality because both sides are non-negative, yields

$$|\mathbf{h}_u^H \mathbf{w}_u| \geq \sqrt{\bar{\gamma}_u} \left(\sum_{\ell\in\mathcal{U},\ell\neq u} |\mathbf{h}_u^H \mathbf{w}_\ell|^2 + \sigma_u^2 \right)^{\frac{1}{2}}, \quad \forall u \in \mathcal{U}. \tag{6.9}$$

The square-root operation preserves the inequality because both sides of (6.8) are non-negative. Since the phase of $\mathbf{w}_u$ does not affect the SINR, we can rotate $\mathbf{w}_u$ such that

$$\Im\{\mathbf{h}_u^H \mathbf{w}_u\} = 0, \quad \Re\{\mathbf{h}_u^H \mathbf{w}_u\} \geq 0. \tag{6.10}$$

Under (6.10), we have $|\mathbf{h}_u^H \mathbf{w}_u| = \Re\{\mathbf{h}_u^H \mathbf{w}_u\}$. Therefore, (6.9) is equivalently transformed

into the second-order cone (SOC) constraint

$$\left\| \begin{bmatrix} \{\mathbf{h}_u^H \mathbf{w}_\ell\}_{\ell \in \mathcal{U}, \ell \neq u} \\ \sigma_u \end{bmatrix} \right\|_2 \leq \frac{1}{\sqrt{\bar{\gamma}_u}} \Re\{\mathbf{h}_u^H \mathbf{w}_u\}, \quad \forall u \in \mathcal{U}. \tag{6.11}$$

Therefore, for fixed SINR targets, the beamforming problem is converted into the following convex SOCP:

$$\mathbf{P3.1}: \quad \min_{\{\mathbf{w}_u\}} \quad \sum_{u \in \mathcal{U}} \|\mathbf{w}_u\|_2^2 \tag{6.12a}$$

$$\text{s.t.} \quad \overline{\text{B1}}: \quad \left\| \begin{bmatrix} \{\mathbf{h}_u^H \mathbf{w}_\ell\}_{\ell \in \mathcal{U}, \ell \neq u} \\ \sigma_u \end{bmatrix} \right\|_2 \leq \frac{1}{\sqrt{\bar{\gamma}_u}} \Re\{\mathbf{h}_u^H \mathbf{w}_u\}, \quad \forall u \in \mathcal{U}, \tag{6.12b}$$

$$\overline{\text{B2}}: \quad \Im\{\mathbf{h}_u^H \mathbf{w}_u\} = 0, \quad \Re\{\mathbf{h}_u^H \mathbf{w}_u\} \geq 0, \quad \forall u \in \mathcal{U}, \tag{6.12c}$$

$$\overline{\text{B3}}: \quad \sum_{u \in \mathcal{U}} \|\mathbf{w}_u\|_2^2 \leq P_{\max}. \tag{6.12d}$$

Therefore, Problem **P3.1** is convex. In particular, it is a standard SOCP and can be efficiently solved using interior-point methods implemented in CVX. After obtaining the beamforming vectors, the achieved SINRs and the original sum-rate objective are recalculated. The update is accepted only if the original objective is non-decreasing.

6.3 IRS Phase Optimization

For fixed beamforming vectors and PA positions, only the IRS reflection vector $\mathbf{v}$ is optimized. According to the far-field channel model, define

$$\mathbf{L}_j = \text{diag}(\mathbf{h}_{r,j}^H)\mathbf{G}, \quad j \in \mathcal{J}. \tag{6.13}$$

Then, the effective far-field channel of user j is

$$\mathbf{h}_{F,j}^H = \mathbf{h}_{d,j}^H + \mathbf{v}^H \mathbf{L}_j. \tag{6.14}$$

Substituting (6.14) into the far-field SINR gives

$$\text{SINR}_{F,j}(\mathbf{v}) = \frac{S_j(\mathbf{v})}{I_j(\mathbf{v})}, \tag{6.15}$$

where the desired signal power is

$$S_j(\mathbf{v}) = |(\mathbf{h}_{d,j}^H + \mathbf{v}^H \mathbf{L}_j)\mathbf{w}_j|^2, \tag{6.16}$$

and the interference-plus-noise power is

$$I_j(\mathbf{v}) = \sum_{m\in\mathcal{J},m\neq j} |(\mathbf{h}_{d,j}^H + \mathbf{v}^H\mathbf{L}_j)\mathbf{w}_m|^2 + \sum_{k\in\mathcal{K}} |(\mathbf{h}_{d,j}^H + \mathbf{v}^H\mathbf{L}_j)\mathbf{w}_k|^2 + \sigma_j^2. \tag{6.17}$$

The achievable rate of far-field user j can then be represented by a difference-of-concave (DC) function:

$$R_{F,j}(\mathbf{v}) = \log_2\left(S_j(\mathbf{v}) + I_j(\mathbf{v})\right) - \log_2\left(I_j(\mathbf{v})\right). \tag{6.18}$$

For notational clarity, define

$$f_j(\mathbf{v}) = \log_2\left(S_j(\mathbf{v}) + I_j(\mathbf{v})\right), \quad g_j(\mathbf{v}) = \log_2\left(I_j(\mathbf{v})\right). \tag{6.19}$$

Then, (6.18) can be compactly written as $R_{F,j}(\mathbf{v}) = f_j(\mathbf{v}) - g_j(\mathbf{v})$. This DC reformulation separates the total received power term from the interference-plus-noise term and provides the basis for the following SCA-based convex approximation.

To decouple the signal and interference terms, introduce slack variables η_j and μ_j satisfying

$$\eta_j \leq S_j(\mathbf{v}), \quad \forall j \in \mathcal{J}, \tag{6.20}$$

and

$$\mu_j \geq I_j(\mathbf{v}), \quad \forall j \in \mathcal{J}. \tag{6.21}$$

The introduction of these auxiliary variables decouples the desired signal power from the interference term, thereby facilitating the subsequent convex approximation. With these variables, the far-field rate can be lower-bounded by the following slack-variable expression:

$$\log_2(\eta_j + \mu_j) - \log_2(\mu_j). \tag{6.22}$$

Accordingly, the original far-field QoS requirement can be conservatively transformed into

$$\log_2(\eta_j + \mu_j) - \log_2(\mu_j) \geq R_{\min}^F, \quad \forall j \in \mathcal{J}. \tag{6.23}$$

However, (6.20) is non-convex because $S_j(\mathbf{v})$ is a convex quadratic function and appears on the right-hand side of a lower-bound constraint. To handle this, define

$$S_j(\mathbf{v}) = |\mathbf{a}_j^H\mathbf{v} + b_j|^2, \tag{6.24}$$

where $\mathbf{a}_j = \mathbf{L}_j\mathbf{w}_j$ and $b_j = \mathbf{h}_{d,j}^H\mathbf{w}_j$. For any feasible point $\mathbf{v}^{(t)}$, the gradient of $S_j(\mathbf{v})$ with respect to $\mathbf{v}$ is

$$\nabla_{\mathbf{v}} S_j(\mathbf{v}^{(t)}) = 2\mathbf{a}_j\left(\mathbf{a}_j^H\mathbf{v}^{(t)} + b_j\right). \tag{6.25}$$

Since a convex quadratic function is globally lower-bounded by its first-order Taylor ex-

pansion, the following lower bound holds:

$$S_j(\mathbf{v}) \geq S_j(\mathbf{v}^{(t)}) + 2\Re\left\{\left(\mathbf{a}_j(\mathbf{a}_j^H\mathbf{v}^{(t)} + b_j)\right)^H(\mathbf{v} - \mathbf{v}^{(t)})\right\} \triangleq \widehat{S}_j(\mathbf{v}; \mathbf{v}^{(t)}). \tag{6.26}$$

Thus, the non-convex constraint (6.20) is replaced by the convex constraint

$$\eta_j \leq \widehat{S}_j(\mathbf{v}; \mathbf{v}^{(t)}), \quad \forall j \in \mathcal{J}. \tag{6.27}$$

In addition, the term $-\log_2(\mu_j)$ in (6.22) is convex in μ_j. Its gradient at $\mu_j^{(t)}$ is $-1/(\mu_j^{(t)} \ln 2)$, and its first-order lower bound is

$$-\log_2(\mu_j) \geq -\log_2(\mu_j^{(t)}) - \frac{\mu_j - \mu_j^{(t)}}{\mu_j^{(t)} \ln 2}. \tag{6.28}$$

Replacing (6.20) and (6.23) with the convex surrogate constraints obtained from (6.27) and (6.28), the IRS phase optimization subproblem at SCA iteration t is approximated as

$$\mathbf{P4}: \quad \max_{\mathbf{v}, \{\eta_j, \mu_j\}} \quad \sum_{j \in \mathcal{J}} \left[\log_2(\eta_j + \mu_j) - \log_2(\mu_j^{(t)}) - \frac{\mu_j - \mu_j^{(t)}}{\mu_j^{(t)} \ln 2}\right] \tag{6.29a}$$

$$\text{s.t.} \quad \text{I1}: \quad \eta_j \leq \widehat{S}_j(\mathbf{v}; \mathbf{v}^{(t)}), \quad \forall j \in \mathcal{J}, \tag{6.29b}$$

$$\text{I2}: \quad \mu_j \geq I_j(\mathbf{v}), \quad \forall j \in \mathcal{J}, \tag{6.29c}$$

$$\text{I3}: \quad \log_2(\eta_j + \mu_j) - \log_2(\mu_j^{(t)}) - \frac{\mu_j - \mu_j^{(t)}}{\mu_j^{(t)} \ln 2} \geq R_{\min}^F, \quad \forall j \in \mathcal{J}, \tag{6.29d}$$

$$\text{I4}: \quad |v_n| \leq 1, \quad n = 1, \ldots, N_i. \tag{6.29e}$$

After replacing the non-convex terms by their first-order surrogate functions, **P4** becomes a standard convex optimization problem and can be efficiently solved using interior-point methods implemented in CVX. After solving **P4**, the passive IRS phase vector is recovered by projection to satisfy the original unit-modulus constraint C4:

$$v_n \leftarrow e^{j \arg(v_n)}, \quad n = 1, \ldots, N_i. \tag{6.30}$$

The original objective is then evaluated using the projected vector. If the sum rate decreases, the previous feasible point is retained. The constructed surrogate function is tight at the current iterate and globally lower-bounds the original rate expression. Therefore, the SCA update provides a non-decreasing improvement when the surrogate solution is accepted according to the original objective value.

6.4 PA Position Optimization

For fixed beamforming vectors and IRS reflection vector, the PA positions determine the near-field effective channel. The PA position optimization problem can be written as

$$\mathbf{P5}: \quad \max_{\{x_n^{\mathrm{PA}}\}} \quad \sum_{k\in\mathcal{K}} R_{N,k}(\mathbf{x}) \tag{6.31a}$$

$$\text{s.t.} \quad \text{A1}: \quad R_{N,k}(\mathbf{x}) \geq R_{\min}^{N}, \quad \forall k \in \mathcal{K}, \tag{6.31b}$$

$$\text{A2}: \quad 0 \leq x_n^{\mathrm{PA}} \leq L, \quad n = 1, \ldots, N_p. \tag{6.31c}$$

Problem **P5** is non-convex because $R_{N,k}(\mathbf{x})$ depends on the PA positions through both the amplitude and phase of the spherical-wave channel. According to the spherical-wave PA channel model, the scalar channel from PA n to near-field user k is

$$a_{k,n}^{\mathrm{PA}}(x_n^{\mathrm{PA}}) = \frac{\sqrt{\eta}}{d_{k,n}} \exp\left(-j\frac{2\pi}{\lambda} d_{k,n} - j\frac{2\pi}{\lambda_g} x_n^{\mathrm{PA}} - \alpha_D x_n^{\mathrm{PA}}\right), \tag{6.32}$$

where

$$d_{k,n} = \sqrt{(x_n^{\mathrm{PA}} - x_k)^2 + y_k^2 + z_k^2}. \tag{6.33}$$

The PA-assisted effective channel is

$$\mathbf{h}_{\mathrm{PA},k}^{H} = \sum_{n=1}^{N_p} a_{k,n}^{\mathrm{PA}}(x_n^{\mathrm{PA}}) \mathbf{g}_n^{H}. \tag{6.34}$$

Thus, the near-field effective channel is

$$\mathbf{h}_{N,k}^{H} = \mathbf{h}_{d,k}^{H} + \mathbf{h}_{\mathrm{PA},k}^{H}. \tag{6.35}$$

Substituting (6.35) into the near-field SINR gives

$$\mathrm{SINR}_{N,k}(\mathbf{x}) = \frac{S_{N,k}(\mathbf{x})}{I_{N,k}(\mathbf{x})}, \tag{6.36}$$

where $\mathbf{x} = [x_1^{\mathrm{PA}}, \ldots, x_{N_p}^{\mathrm{PA}}]^T$,

$$S_{N,k}(\mathbf{x}) = |\mathbf{h}_{N,k}^{H}(\mathbf{x})\mathbf{w}_k|^2, \tag{6.37}$$

and

$$I_{N,k}(\mathbf{x}) = \sum_{i\in\mathcal{K}, i\neq k} |\mathbf{h}_{N,k}^{H}(\mathbf{x})\mathbf{w}_i|^2 + \sum_{j\in\mathcal{J}} |\mathbf{h}_{N,k}^{H}(\mathbf{x})\mathbf{w}_j|^2 + \sigma_k^2. \tag{6.38}$$

Accordingly, the achievable rate of near-field user k can be written in the same DC form as the IRS-assisted far-field rate:

$$R_{N,k}(\mathbf{x}) = \log_2\left(S_{N,k}(\mathbf{x}) + I_{N,k}(\mathbf{x})\right) - \log_2\left(I_{N,k}(\mathbf{x})\right). \tag{6.39}$$

Define

$$F_k(\mathbf{x}) = \log_2\left(S_{N,k}(\mathbf{x}) + I_{N,k}(\mathbf{x})\right), \quad G_k(\mathbf{x}) = \log_2\left(I_{N,k}(\mathbf{x})\right). \tag{6.40}$$

Then, $R_{N,k}(\mathbf{x}) = F_k(\mathbf{x}) - G_k(\mathbf{x})$. This reformulation shows that the PA position optimization has the same DC structure as the IRS phase optimization, but the non-convexity now originates from the position-dependent spherical-wave channel. Following the same DC reformulation and SCA framework developed for the IRS optimization, the PA position optimization can also be transformed into a sequence of convex optimization problems, introduce slack variables $\eta_{N,k}$ and $\mu_{N,k}$:

$$\eta_{N,k} \le S_{N,k}(\mathbf{x}), \quad \mu_{N,k} \ge I_{N,k}(\mathbf{x}). \tag{6.41}$$

Then the near-field rate is lower-bounded by

$$\log_2(\eta_{N,k} + \mu_{N,k}) - \log_2(\mu_{N,k}). \tag{6.42}$$

Consequently, the original near-field QoS constraint A1 in **P5** can be conservatively represented as

$$\log_2(\eta_{N,k} + \mu_{N,k}) - \log_2(\mu_{N,k}) \ge R_{\min}^N, \quad \forall k \in \mathcal{K}. \tag{6.43}$$

To construct a local convex approximation, first linearize the distance function around $x_n^{\mathrm{PA},(t)}$:

$$d_{k,n} \approx d_{k,n}^{(t)} + \frac{x_n^{\mathrm{PA},(t)} - x_k}{d_{k,n}^{(t)}}\left(x_n^{\mathrm{PA}} - x_n^{\mathrm{PA},(t)}\right). \tag{6.44}$$

The derivative of (6.32) with respect to x_n^{PA} is

$$\frac{\partial a_{k,n}^{\mathrm{PA}}}{\partial x_n^{\mathrm{PA}}} = a_{k,n}^{\mathrm{PA}}\left[-\frac{1}{d_{k,n}}\frac{\partial d_{k,n}}{\partial x_n^{\mathrm{PA}}} - j\frac{2\pi}{\lambda}\frac{\partial d_{k,n}}{\partial x_n^{\mathrm{PA}}} - j\frac{2\pi}{\lambda_g} - \alpha_D\right], \tag{6.45}$$

where

$$\frac{\partial d_{k,n}}{\partial x_n^{\mathrm{PA}}} = \frac{x_n^{\mathrm{PA}} - x_k}{d_{k,n}}. \tag{6.46}$$

Therefore, using (6.45), the effective near-field channel becomes an affine approximation around the current PA position:

$$\mathbf{h}_{N,k}^H(\mathbf{x}) \approx \widehat{\mathbf{h}}_{N,k}^H(\mathbf{x};\mathbf{x}^{(t)}) = \mathbf{h}_{N,k}^H(\mathbf{x}^{(t)}) + \sum_{n=1}^{N_p}\left.\frac{\partial \mathbf{h}_{N,k}^H}{\partial x_n^{\mathrm{PA}}}\right|_{\mathbf{x}^{(t)}}\left(x_n^{\mathrm{PA}} - x_n^{\mathrm{PA},(t)}\right). \tag{6.47}$$

Then, for the desired signal term $|\widehat{\mathbf{h}}_{N,k}^H(\mathbf{x};\mathbf{x}^{(t)})\mathbf{w}_k|^2$, the affine approximation in (6.47) is first substituted into the received signal expression. Then, the following first-order

quadratic lower bound is used:

$$S_{N,k}(\mathbf{x}) \geq S_{N,k}(\mathbf{x}^{(t)}) + 2\Re\left\{\left(\mathbf{h}_{N,k}^H(\mathbf{x}^{(t)})\mathbf{w}_k\right)^* \left[\widehat{\mathbf{h}}_{N,k}^H(\mathbf{x};\mathbf{x}^{(t)})\mathbf{w}_k - \mathbf{h}_{N,k}^H(\mathbf{x}^{(t)})\mathbf{w}_k\right]\right\} \triangleq \widehat{S}_{N,k}(\mathbf{x};\mathbf{x}^{(t)}). \tag{6.48}$$

The convex term $-\log_2(\mu_{N,k})$ is also lower-bounded as

$$-\log_2(\mu_{N,k}) \geq -\log_2(\mu_{N,k}^{(t)}) - \frac{\mu_{N,k} - \mu_{N,k}^{(t)}}{\mu_{N,k}^{(t)} \ln 2}. \tag{6.49}$$

The constructed surrogate is tight at the current PA position and lower-bounds the original near-field rate. Hence, replacing the non-convex signal constraint and the QoS constraint derived from A1 by their corresponding first-order surrogate functions . Therefore, the PA position optimization subproblem is approximated as

$$\mathbf{P5.1}: \quad \max_{\mathbf{x},\{\eta_{N,k},\mu_{N,k}\}} \quad \sum_{k\in\mathcal{K}} \left[\log_2(\eta_{N,k}+\mu_{N,k}) - \log_2(\mu_{N,k}^{(t)}) - \frac{\mu_{N,k}-\mu_{N,k}^{(t)}}{\mu_{N,k}^{(t)}\ln 2}\right] \tag{6.50a}$$

$$\text{s.t.} \quad \overline{\text{A1}}: \quad \eta_{N,k} \leq \widehat{S}_{N,k}(\mathbf{x};\mathbf{x}^{(t)}), \quad \forall k \in \mathcal{K}, \tag{6.50b}$$

$$\overline{\text{A2}}: \quad \mu_{N,k} \geq \widehat{I}_{N,k}(\mathbf{x};\mathbf{x}^{(t)}), \quad \forall k \in \mathcal{K}, \tag{6.50c}$$

$$\overline{\text{A3}}: \quad \log_2(\eta_{N,k}+\mu_{N,k}) - \log_2(\mu_{N,k}^{(t)}) - \frac{\mu_{N,k}-\mu_{N,k}^{(t)}}{\mu_{N,k}^{(t)}\ln 2} \geq R_{\min}^N, \quad \forall k \in \mathcal{K}, \tag{6.50d}$$

$$\overline{\text{A4}}: \quad 0 \leq x_n^{\text{PA}} \leq L, \quad n = 1,\ldots,N_p. \tag{6.50e}$$

Here, $\widehat{I}_{N,k}$ is obtained by substituting the affine channel approximation in (6.47) into the interference expression. Therefore, the surrogate optimization problem **P5.1** is a convex problem and can be easily solved using convex optimization solvers. The obtained PA positions are then substituted back into the original problem to evaluate the true objective value before the AO algorithm proceeds to the next iteration.

6.5 Overall AO Algorithm

The overall alternating optimization process is outlined in Algorithm 1. The optimization variables are initialized by feasible or randomly generated points. At each outer iteration, the beamforming, IRS phase, and PA position subproblems are updated sequentially. The original objective value is evaluated after each outer iteration. The AO procedure terminates when the relative objective improvement satisfies

$$\frac{\left|R_{\text{sum}}^{(\tau+1)} - R_{\text{sum}}^{(\tau)}\right|}{R_{\text{sum}}^{(\tau)}} \leq \epsilon \tag{6.51}$$

or when the maximum iteration number $\tau_{\max}$ is reached.

Algorithm 1 AO Algorithm for the IRS-Assisted PA System

1: Specify the maximum iteration number $\tau_{\max}$ and tolerance ϵ, initialize $\tau = 0$, and initialize $\{\mathbf{w}_u^{(\tau)}\}$, $\mathbf{v}^{(\tau)}$, and $\{x_n^{\mathrm{PA},(\tau)}\}$.
2: **repeat** ▷ Main Loop: AO
3: Update $\{\mathbf{w}_u^{(\tau+1)}\}$ by solving **P3.1** with fixed $\mathbf{v}^{(\tau)}$ and $\{x_n^{\mathrm{PA},(\tau)}\}$.
4: Obtain $\mathbf{v}^{(\tau+1)}$ by solving **P4** with fixed $\{\mathbf{w}_u^{(\tau+1)}\}$ and $\{x_n^{\mathrm{PA},(\tau)}\}$, followed by the projection in (6.30).
5: Obtain $\{x_n^{\mathrm{PA},(\tau+1)}\}$ by solving **P5.1** with fixed $\{\mathbf{w}_u^{(\tau+1)}\}$ and $\mathbf{v}^{(\tau+1)}$.
6: Compute the original sum-rate objective. If the objective value decreases, keep the previous feasible variables.
7: Set $\tau = \tau + 1$.
8: **until** the relative objective improvement satisfies (6.51) or the maximum iteration number is reached.

6.6 Convergence Analysis

Although the resulting problem is non-convex, the proposed approach will yield a feasible point in each iteration step. In each iteration step, only one group of optimization variables is optimized, while the other variables stay the same.

Namely, the transmit beamforming vectors, the IRS phase shifters, and the PA positions are optimized successively. As each sub-problem is solved without decreasing the objective function, the resulting system sum rate satisfies the following monotonic relationship

$$R_{\mathrm{sum}}^{(0)} \leq R_{\mathrm{sum}}^{(1)} \leq \cdots \leq R_{\mathrm{sum}}^{(\tau)}. \tag{6.52}$$

Also, the objective function does not tend towards infinity as the feasible solution space is bounded and the transmit power of BS is bounded too. Thus, the sequence of objectives formed is monotonically non-decreasing and is upper bounded.

Due to the convergence nature of alternating optimization technique and successively convex approximation, the new method can be assured to converge to a stationary point of the problem.

6.7 Complexity Analysis

Let $U = |\mathcal{U}| = K + J$ denote the total number of users. The beamforming subproblem **P3.1** is an SOCP with approximately MU complex beamforming variables and U SOC

constraints. If an interior-point solver is used, its worst-case complexity can be represented as

$$\mathcal{O}\left(I_{\mathrm{BF}}(MU)^3\right), \tag{6.53}$$

where I_{BF} denotes the number of inner solver iterations.

For the IRS phase update, the SCA subproblem **P4** contains N_i complex IRS variables and $2J$ real slack variables. Let I_{IRS} denote the number of SCA iterations for the IRS block. The corresponding complexity is approximately

$$\mathcal{O}\left(I_{\mathrm{IRS}}(N_i + 2J)^3\right). \tag{6.54}$$

For the PA position update, if the SCA formulation **P5.1** is adopted, the complexity is approximately

$$\mathcal{O}\left(I_{\mathrm{PA}}(N_p + 2K)^3\right), \tag{6.55}$$

where I_{PA} is the number of PA SCA iterations. In the simulation code, the PA positions are updated by grid search. If G_{PA} grid points are used for each PA, the PA search complexity is

$$\mathcal{O}\left(N_p G_{\mathrm{PA}} K\right), \tag{6.56}$$

excluding the constant cost of channel reconstruction.

In addition, the simulation uses a discrete phase search for the IRS update. If G_ϕ candidate phases are tested for each IRS element, the practical IRS search complexity is approximately

$$\mathcal{O}\left(N_i G_\phi J M\right), \tag{6.57}$$

because each candidate phase requires evaluating the far-field effective channel gain. Therefore, when the SCA-based PA update is used, the total complexity of the AO algorithm can be summarized as

$$\mathcal{O}\left(T_{\mathrm{AO}}\left(I_{\mathrm{BF}}(MU)^3 + I_{\mathrm{IRS}}(N_i + 2J)^3 + I_{\mathrm{PA}}(N_p + 2K)^3\right)\right), \tag{6.58}$$

where T_{AO} is the number of AO iterations. For the grid-search implementation used in the simulations, the PA term can be replaced by $N_p G_{\mathrm{PA}} K$, yielding

$$\mathcal{O}\left(T_{\mathrm{AO}}\left(I_{\mathrm{BF}}(MU)^3 + I_{\mathrm{IRS}}(N_i + 2J)^3 + N_p G_{\mathrm{PA}} K\right)\right). \tag{6.59}$$

This expression shows that the computational complexity increases polynomially with the numbers of BS antennas, IRS elements, PAs, and users, which is significantly lower than joint exhaustive search over all beamforming vectors, IRS phases, and PA positions.

6.8 Simulation Setup

In order to analyze the effectiveness of the developed resource allocation algorithm, numerical simulation is conducted using MATLAB based on Monte Carlo simulation techniques. If not stated otherwise, all the simulation results have been carried out under a normalized narrowband channel model. As a result, no particular carrier frequency or waveguide dielectric is considered in the simulation.The large-scale propagation effects are represented by the reference channel gain β_0, the path-loss exponent α, the direct-link gain, and the IRS-link gain. Likewise, the guided wavelength λ_g and the dielectric attenuation coefficient α_D appearing in the general physical channel model are not explicitly evaluated in the current MATLAB implementation.The IRS is modeled as an ideal lossless passive surface. Hence, the amplitude reflection coefficient of each IRS element is fixed as $\beta_n = 1$, while the phase responses remain the only optimization variables.

To ensure reproducibility, the random number generator is initialized using `rng(3)`.Unless otherwise pointed, the simulation parameters in all experiments remain unchanged. The BS is equipped with $M = 16$ antennas and simultaneously serves $K = 6$ near-field users together with $J = 2$ far-field users. The system deploys $N_p = 4$ movable pinching antennas and an IRS containing $N_i = 64$ reflecting elements.The transmit power budget is set to $P_{\max} = 15$ dBm, while the noise power equals 5×10^{-9}. The reference channel gain and path-loss exponent are selected as $\beta_0 = 10^{-4}$ and $\alpha = 2$. Each dielectric waveguide has a movement range of $L_{\mathrm{PA}} = 10$ m. The number of Monte Carlo channel realizations is 50. The PA grid contains $G_{\mathrm{PA}} = 100$ candidate positions, and the IRS phase grid contains $G_\phi = 24$ candidate phase values. The 24 candidate IRS phases are uniformly sampled over $[0, 2\pi)$, which offers a good balance between computational complexity and phase-search accuracy.

Table 6.1: Default Simulation Configuration

Parameter	Value
BS antenna count, M	16
Near-field user count, K	6
Far-field user count, J	2
Number of PAs, N_p	4
IRS reflecting elements, N_i	64
BS transmit power limit, $P_{\max}$	15 dBm
Noise power, σ^2	5×10^{-9}
Reference channel gain, β_0	10^{-4}
Path-loss exponent, α	2
PA movement range, L	10 m
Monte Carlo realizations	50
PA grid size, G_{PA}	100
IRS phase grid size, G_ϕ	24
Direct-link gain	10^{-7}
IRS-link gain	6×10^{-5}
Channel model	Normalized narrowband model
Specific carrier frequency	Not explicitly imposed
Waveguide material	Not explicitly specified
IRS amplitude reflection coefficient, β_n	1

In each Monte Carlo realization, the near-field users are generated with x-coordinates uniformly spaced from 2 m to 8 m and random y-coordinates in $[1, 3]$ m. The far-field users are generated with x-coordinates uniformly spaced from 20 m to 30 m and random y-coordinates in $[15, 20]$ m. The direct BS-user channels, BS-IRS channel, IRS-user channels, and BS-PA feeding channels are generated as independent Rayleigh fading channels with the corresponding large-scale gains. The direct link gain is set to 10^{-7}, and the IRS-related channel gain is set to 6×10^{-5}.

For each channel realization, the simulation follows the same AO logic as Algorithm 1:

1. Generate near-field and far-field user locations.
2. Generate the direct BS-user, BS-IRS, IRS-user, and BS-PA feeding channels.
3. Initialize the BS beamforming vectors, IRS reflection vector, and PA positions.
4. Update the beamforming vectors with fixed IRS phases and PA positions.
5. Update the IRS reflection vector with fixed beamforming vectors and PA positions. In the numerical implementation, the IRS phase update is realized through discrete phase search over the uniformly sampled phase grid.

6. Update the PA positions with fixed beamforming vectors and IRS phases. In the numerical implementation, the PA update is realized through grid search over $[0, L]$.

7. Evaluate the original system sum rate and repeat the AO updates until (6.51) is satisfied or the maximum iteration number is reached.

8. Repeat the above procedure for all Monte Carlo realizations and average the obtained sum rates.

6.9 Baseline Schemes

To evaluate the performance gains provided by the movable PAs and the IRS, the following three transmission schemes are considered throughout the numerical evaluation.

- **Proposed IRS-assisted PA scheme:** This technique employs both flexible PAs and IRS. BS beamforming vectors, PA locations, and IRS phase are optimized jointly by the suggested alternating optimization approach. In the numerical study, beamforming vectors for BSs are obtained by employing zero-forcing beamforming, and the position of PAs is optimized through grid search method, while IRS phase shifts are optimized via discrete phase shift search method.

- **PA-only scheme:** In the benchmark configuration, the mobile PAs are retained, but the IRS-enabled reflection channel connection is disabled by assigning the IRS's effect as zero. Optimization of both PAs location and BS beamforming vector is done in a similar manner as in the proposed configuration. This means that the performance difference of the two configurations will illustrate the performance improvement that comes from having an IRS.

- **Conventional BS scheme:** The benchmark will disable the PA help and IRS reflecting capabilities. The users will use only the regular BS-user connection and the BS beamforming vector will be calculated using the zero-forcing technique. In essence, it becomes the conventional multiple users MISO transmissions system where there are no reconfigurable propagation components.

All the schemes employ the same set of user locations, channel realizations, transmit power budget, noise power, and beamforming technique in order to make a fair comparison. Average system sum rate (in bps/Hz) is taken as the performance metric. These metrics can be used to evaluate the contribution of PA and IRS schemes individually.

6.10 Numerical Results

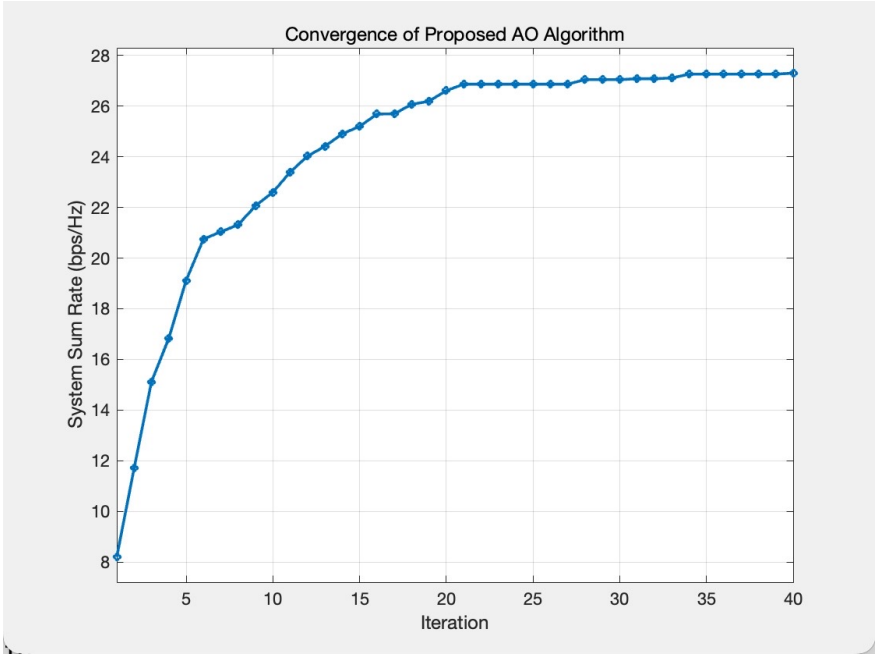

Figure 6.1: Convergence performance of the AO algorithm.

Fig. 6.1 shows the convergence of the proposed AO algorithm under the default simulation configuration.The system sum rate has gone up rapidly during the first several iterations, because the initial beamforming vectors, IRS phases, and PA positions are still far from a favorable local solution. After about 20 iterations, the improvement becomes much smaller and the curve gradually approaches a stable value. This confirms that the accepted AO updates generate a non-decreasing objective sequence and that the stopping criterion in (6.51) is appropriate for the considered simulation setup.

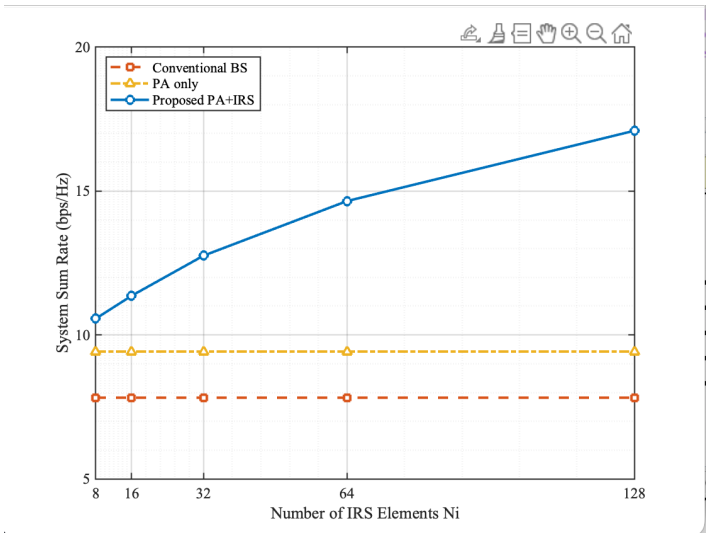

Figure 6.2: IRS reflecting elements N_i on the achievable system sum rate.

Fig. 6.2 updates the average system sum rate achieved by the three benchmark schemes when the number of IRS reflecting elements varies from $N_i \in \{8, 16, 32, 64, 128\}$. As more reflecting elements are deployed, the proposed IRS-assisted PA scheme continuously improves its achievable sum rate. This improvement arises from the extra passive beamforming capabilities offered by the increased size of the IRS and hence improved BS-IRS-user channel cascade especially for far-field users. In contrast, the performance of the traditional BS and the PA-only baseline is almost identical since neither of these techniques benefits from the phase optimization capabilities of the IRS. It is noted that the performance improvement tends to level off as N_i increases. This is due to the fact that the transmit power is constant and hence the passive beamforming capability available would be limited by the multi-user interference and QoS constraints. These observations further validate the effectiveness of the proposed AO-based IRS phase optimization strategy presented in Section 6.3.

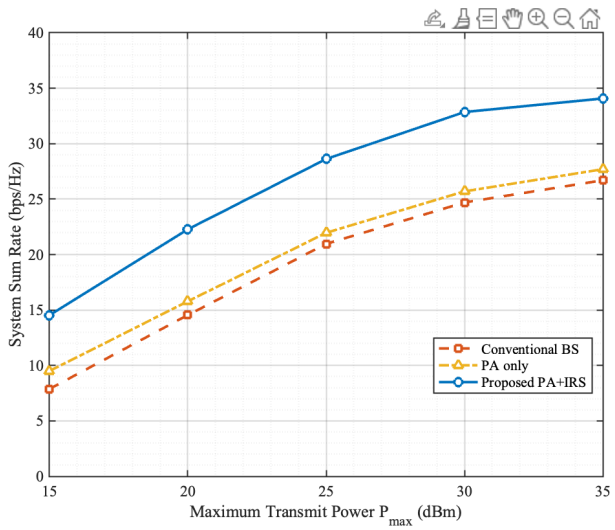

Figure 6.3: Effect of the transmit power $P_{\max}$ on the system sum rate.

Fig. 6.3 compares the average system sum rates of the proposed and baseline schemes for different maximum BS transmit-power budgets, $P_{\max} \in \{15, 20, 25, 30, 35\}$ dBm. The total sum rate for all schemes improves with respect to $P_{\max}$ since an increase in transmit-power budget leads to an improvement in the received SINR. It has been observed that the IRS-assisted PA-based technique works much better than the two other techniques because of the positive effect of the movable PAs on the near-field channels and IRS usage on the far-field reflected channels. As can be seen from the simulations, the gap between the two schemes grows when the transmit power is increased. It has been also noticed that the slope of the curves decreases for very high values of transmit power as the system is more affected by interference and spatial channels than just thermal noise. This behavior is related to the beamforming update in Section 6.2, where the available transmit power is allocated under fixed interference and QoS constraints.

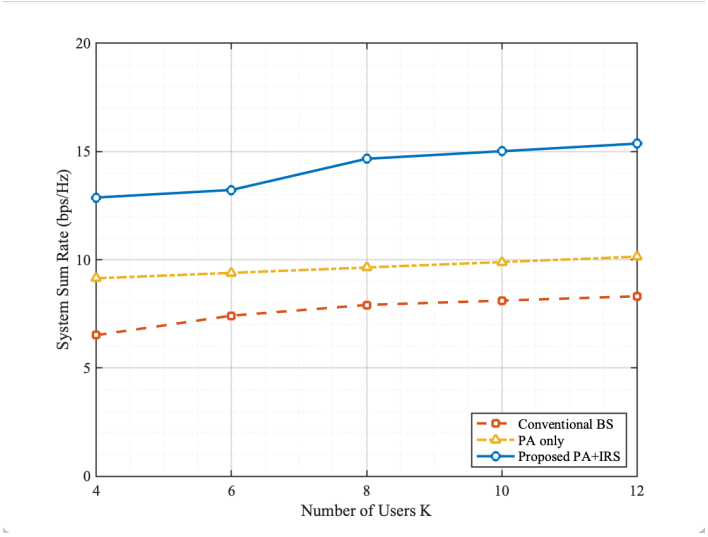

Figure 6.4: System sum rate under different total numbers of users K_{total}.

Fig. 6.4 depicts the average system sum rate as the total number of users varies over $K_{\text{total}} \in \{4, 6, 8, 10, 12\}$. For each simulation, around 75% of the users belong to the near-field area, whereas the other users act as far-field users. The rate sum gets better as more users come in because all the additional users will add to the sum of the rate. However, the increase rate of sum is sub-linear because the transmit power remains constant, but there is more interference among the users because of more users being served. The PA with IRS provides the best sum rate due to improvement in the near and far field communication. The slower growth rate for more users is because of the sharing of the same power by many users and also due to more interference generated.

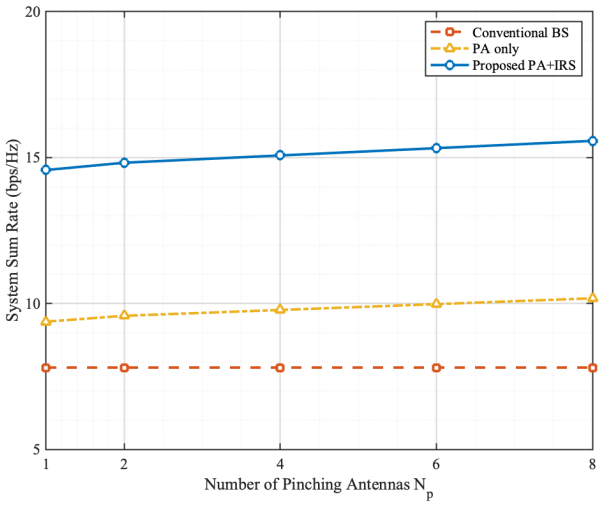

Figure 6.5: Influence of the amount of pinching antennas N_p on the achievable system sum rate.

Fig. 6.5 compares the average system sum rates of the three schemes for different numbers of movable PAs, $N_p \in \{1, 2, 4, 6, 8\}$. Increasing N_p provides more movable radiation

points and therefore improves the near-field channel quality. As a result, the PA-only scheme achieves a gradual sum-rate increase. The proposed IRS-assisted PA scheme also improves with N_p and remains above the PA-only baseline because it further benefits from the IRS-assisted far-field reflected channel. The conventional BS scheme is nearly constant because it does not use movable PAs and is therefore insensitive to N_p. The gain from increasing N_p becomes marginal when the number of PAs is sufficiently large, since the near-field spatial diversity has already been largely exploited and the remaining performance is limited by transmit power and interference. This validates the effectiveness of the PA position optimization developed in Section 6.4.

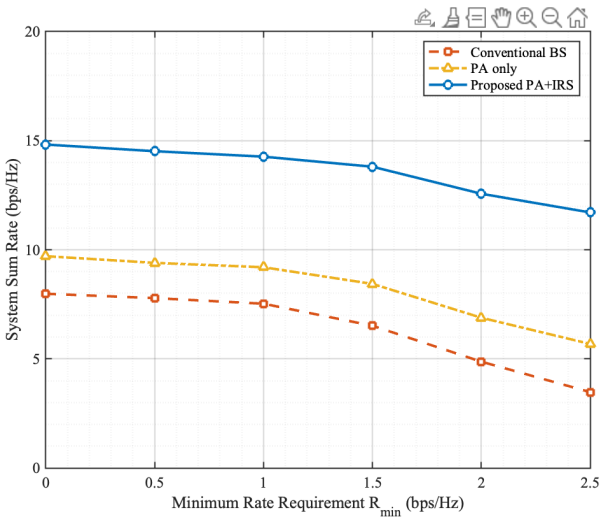

Figure 6.6: System sum rate under different minimum QoS rate requirements $R_{\min}$.

Fig. 6.6 compares the average system sum rates of the three schemes as the minimum QoS rate requirement varies over $R_{\min} \in \{0, 0.5, 1, 1.5, 2, 2.5\}$ bps/Hz. As $R_{\min}$ increases, the feasible set becomes smaller because every user must satisfy a stricter minimum-rate constraint. Thus, the attainable sum rate reduces for all the schemes. However, the IRS-aided PA scheme attains the maximum rate since its joint optimization of PA and IRS phases results in a higher level of channel improvement and robustness to QoS constraints. Increasing $R_{\min}$ reduces the feasible region of the optimization problem, leaving fewer degrees of freedom for maximizing the system sum rate after all users' QoS requirements are satisfied. This behavior is consistent with the QoS-constrained formulations in the original constraints C1 and C2, as well as their transformed counterparts in $\widetilde{\text{C1}}$, $\widetilde{\text{C2}}$, I3, and $\overline{\text{A3}}$.

In general, the numerical results show that the IRS-aided PA system outperforms both the traditional BS and the PA-only baseline approaches. This improvement is achieved due to the synergistic effects of the two reconfigurable devices. The position-movable PAs help with near-field transmissions by adjusting the radiation points on the waveguide, while the IRS contributes to the far-field transmissions by regulating the propagation

path. The results confirm the feasibility of the proposed joint resource allocation scheme under the power budget, QoS, IRS unit modulus, and PA mobility constraints.

Chapter 7

Conclusion and Future Work

7.1 Conclusion

In this paper, we tackle the simultaneous problem of resource allocation for IRS assisted pinching antennas communication systems where both the near-field channel and far-field channel are present. Firstly, we formulate an entire communication system model, where apart from the direct communication links between BS and users, near-field PA aided and far-field IRS aided communication channels are taken into account.

The non-convex formulation of the problem is carried out by formulating the optimization problem in terms of the maximization of the sum rate of the system with the transmit power, QoS, unit modulus constraints of IRS elements and PA moving constraints.

Alternating optimization algorithm is applied to resolve the non-convex optimization issue through subdividing it into three problems and solving each one separately. Specifically, the beamforming problem is transformed into the second-order cone programming problem, the IRS phase shifting problem is optimized through the method of successive convex approximation, and the PA location problem is optimized via convex surrogate approximation of the near-field channel model.

According to the theoretical analysis and simulation, it can be concluded that the proposed resource allocation scheme is able to achieve the mean system throughput under all the practical requirements of the system.

Moreover, the IRS phase shifting schemes and the locations of the power amplifiers can provide some flexibility regarding space utilization, which leads to the enhanced near field and far field communications. As compared with the selected base case, the IRS assisted shrinking antenna system performs better.

Finally, this work presents an optimization model for IRS-assisted shrinking antenna systems, and hence offers some useful insights for the development of the resource allocation scheme for future wireless communication systems.

7.2 Future Work

Despite performance results that have been quite encouraging in this thesis, it is true that there is a need for further research in several areas.

First of all, this thesis takes perfect CSI knowledge as a premise. Further work in this direction might include consideration of imperfect CSI models and analysis of resource allocation algorithms under such conditions.

Secondly, this system considers the use of only one IRS deployment. It is quite interesting to consider whether multiple IRS deployments and multi-cell communications would lead to improved performance.

Moreover, user and PA mobility can be added to the current model of the system. This is an interesting and challenging task of optimizing a system in which both PAs and users move and channels are time-varying.

Finally, machine learning techniques like deep reinforcement learning and neural-network-based resource allocation can be considered as low-complexity techniques for IRS assisted pinching antennas. Another promising direction is blockage-aware resource allocation for pinching antenna systems under realistic propagation environments [64].

These research directions provide great opportunities for generalization of the current system to practical and intelligent 6G wireless communications.

Bibliography

[1] X. Li, Z. Wu, Y. Cai, S. Hu, Y. Liao, and W. Yuan, "Win-win of communication and sensing security for MC-NOMA ISAC systems," *IEEE J. Sel. Areas Commun.*, vol. 43, no. 9, pp. 3214–3230, Sep. 2025.

[2] Y. Cai, Z. Wei, S. Hu, C. Liu, D. W. K. Ng, and J. Yuan, "Resource allocation and 3D trajectory design for power-efficient IRS-assisted UAV-NOMA communications," *IEEE Trans. Wireless Commun.*, vol. 21, no. 12, pp. 10 315–10 334, Dec. 2022.

[3] Y. Zhang, S. Hu, D. Mishra, and D. W. K. Ng, "Movable-antenna array-enhanced energy-efficient RSMA communication networks," in *Proc. IEEE Int. Conf. Commun. (ICC)*, May 2026.

[4] R. Zhao, Y. Zhang, S. Hu, and D. W. K. Ng, "Pinching antenna-assisted ISAC with waveguide mode selection," in *Proc. 20th Int. Symp. Wireless Commun. Syst. (ISWCS)*, Aug. 2026.

[5] T. Shen, X. Wu, Y. Zhan, S. Hu, D. W. K. Ng, and L. Yang, "Environment-aware satellite-terrestrial channel knowledge map," in *Proc. 20th Int. Symp. Wireless Commun. Syst. (ISWCS)*, Aug. 2026.

[6] L. Wang, Y. Cai, X. Li, and S. Hu, "Joint beamforming and port selection for fluid antenna-assisted nearshore ISAC systems," in *Proc. 20th Int. Symp. Wireless Commun. Syst. (ISWCS)*, Aug. 2026.

[7] Z. Zhang, R. Zhao, S. Hu, and D. W. K. Ng, "Energy-efficient resource allocation for six-dimensional movable antenna systems," in *Proc. IEEE 37th Int. Symp. Pers., Indoor Mobile Radio Commun. (PIMRC)*, Sep. 2026.

[8] S. Hu, Z. Wei, Y. Cai, C. Liu, D. W. K. Ng, and J. Yuan, "Robust and secure sum-rate maximization for multiuser MISO downlink systems with self-sustainable IRS," *IEEE Trans. Commun.*, vol. 69, no. 10, pp. 7032–7049, Oct. 2021.

[9] I. F. Akyildiz, A. Kak, and S. Nie, "6g and beyond: The future of wireless communications systems," *IEEE Access*, vol. 8, pp. 133 995–134 030, 2020.

[10] M. Di Renzo, A. Zappone, M. Debbah, M.-S. Alouini, C. Yuen, J. de Rosny, and S. Tretyakov, "Smart radio environments empowered by reconfigurable intelligent surfaces: How it works, state of research, and the road ahead," *IEEE Journal on Selected Areas in Communications*, vol. 38, no. 11, pp. 2450–2525, 2020.

[11] C. Pan, H. Ren, K. Wang, J. F. Kolb, M. Elkashlan, M. Chen, M. Di Renzo, Y. Hao, J. Wang, A. L. Swindlehurst, X. You, and L. Hanzo, "Reconfigurable intelligent surfaces for 6g systems: Principles, applications, and research directions," *IEEE Communications Magazine*, vol. 59, no. 6, pp. 14–20, 2021.

[12] S. Gong, X. Lu, D. T. Hoang, D. Niyato, L. Shu, D. I. Kim, and Y.-C. Liang, "Towards smart wireless communications via intelligent reflecting surfaces: A contemporary survey," *IEEE Communications Surveys & Tutorials*, vol. 22, no. 4, pp. 2283–2314, 2020.

[13] Q. Wu and R. Zhang, "Towards smart and reconfigurable environment: Intelligent reflecting surface aided wireless network," *IEEE Communications Magazine*, vol. 58, no. 1, pp. 106–112, 2020.

[14] E. Bjornson and L. Sanguinetti, "Power scaling laws and near-field behaviors of massive mimo and intelligent reflecting surfaces," *IEEE Open Journal of the Communications Society*, vol. 1, pp. 1306–1324, 2020.

[15] X. Yu, D. Xu, Y. Sun, D. W. K. Ng, and R. Schober, "Robust and Secure Wireless Communications via Intelligent Reflecting Surfaces," *IEEE J. Sel. Areas Commun.*, vol. 38, no. 11, pp. 2637–2652, 2020.

[16] X. Yu, D. Xu, D. W. K. Ng, and R. Schober, "IRS-Assisted Green Communication Systems: Provable Convergence and Robust Optimization," *IEEE Trans. Commun.*, vol. 69, no. 9, pp. 6313–6329, 2021.

[17] Y. Wu, D. Xu, D. W. K. Ng, R. Schober, and W. Gerstacker, "Globally Optimal Resource Allocation Design for Discrete Phase Shift IRS-Assisted Multiuser Networks with Perfect and Imperfect CSI," *IEEE Trans. Wireless Commun.*, vol. 24, pp. 1306–1324, 2025.

[18] M. A. Saeidi, M. J.Emadi, H. Masoumi, M. R. Mili, D. W. K. Ng, and I. Krikidis, "Weighted Sum-Rate Maximization for Multi-IRS-assisted Full-Duplex Systems with Hardware Impairments," *IEEE Trans. Cogn. Commun. Netw.*, vol. 7, no. 2, pp. 466–481, 2021.

[19] R. Long, Y.-C. Liang, Y. Pei, and E. G. Larsson, "Active reconfigurable intelligent surface aided wireless communications," *IEEE Transactions on Wireless Communications*, vol. 20, no. 8, pp. 4962–4975, 2021.

[20] A. Huang, X. Mu, L. Guo, and G. Zhu, "Hybrid active-passive ris transmitter enabled energy-efficient multi-user communications," *arXiv preprint arXiv:2403.01956*, 2024.

[21] Y. Gao, Q. Wu, G. Zhang, W. Chen, D. W. K. Ng, and M. D. Renzo, "Beamforming Optimization for Active Intelligent Reflecting Surface-Aided SWIPT," *IEEE Trans. Wireless Commun.*, vol. 22, no. 1, pp. 362–378, 2023.

[22] D. Xu, V. Jamali, X. Yu, D. W. K. Ng, and R. Schober, "Optimal Resource Allocation Design for Large IRS-Assisted SWIPT Systems: A Scalable Optimization Framework," *IEEE Trans. Commun.*, vol. 70, no. 2, pp. 1423–1441, 2022.

[23] S. Zargari, A. Khalili, Q. Wu, M. R. Mili, and D. W. K. Ng, "Max-Min Fair Energy-efficient Beamforming Design for Intelligent Reflecting Surface-Aided SWIPT Systems with Non-linear Energy Harvesting Model," *IEEE Trans. Veh. Technol.*, vol. 70, no. 6, pp. 5848–5864, 2021.

[24] J. An, C. Xu, Q. Wu, D. W. K. Ng, M. D. Renzo, C. Yuen, and L. Hanzo, "Codebook-Based Solutions for Reconfigurable Intelligent Surfaces and Their Open Challenges," *IEEE Wireless Commun.*, vol. 31, no. 2, pp. 134–141, 2024.

[25] Y. Chu, Z. Wei, Z. Yang, and D. W. K. Ng, "Channel Estimation for RIS-Aided MIMO Systems: A Partially Decoupled Atomic Norm Minimization Approach," *IEEE Trans. Wireless Commun.*, vol. 23, no. 11, pp. 16 048–16 061, 2024.

[26] C. Liu, X. Liu, D. W. K. Ng, and J. Yuan, "Deep Residual Learning for Channel Estimation in Intelligent Reflecting Surface-Assisted Multi-User Communications," *IEEE Trans. Wireless Commun.*, vol. 21, no. 2, pp. 898–912, 2022.

[27] J. Yao, J. Xu, W. Xu, D. W. K. Ng, C. Yuen, and X. You, "Robust Beamforming Design for RIS-aided Cell-free Systems with CSI Uncertainties and Capacity-limited Backhaul," *IEEE Trans. Commun.*, vol. 71, no. 8, pp. 4636–4649, 2023.

[28] E. Shi, J. Zhang, R. He, H. Jiao, Z. Wang, B. Ai, and D. W. K. Ng, "Spatially Correlated Reconfigurable Intelligent Surfaces-Aided Cell-Free Massive MIMO Systems," *IEEE Trans. Veh. Technol.*, vol. 71, no. 8, pp. 9073–9077, 2022.

[29] P. Zhang, J. Zhang, H. Xiao, X. Zhang, D. W. K. Ng, and B. Ai, "Joint Distributed Precoding and Beamforming for RIS-Aided Cell-Free Massive MIMO Systems," *IEEE Trans. Veh. Technol.*, vol. 73, no. 4, pp. 5994–5999, 2024.

[30] Y. Lu, J. Zhang, Y. Zhu, J. Zheng, D. Yang, D. W. K. Ng, and B. Ai, "Performance Optimization of RIS-Aided Cell-Free Massive MIMO Systems With DRL Approach," *IEEE Trans. Wireless Commun.*, vol. 25, pp. 6711–6728, 2026.

[31] E. Shi, Y. Zhu, J. Zhang, Z. Liu, C. Yuen, D. W. K. Ng, M. D. Renzo, and B. Ai, "Joint Precoding and AP Selection for Energy-Efficient RIS-aided Cell-Free Massive MIMO with Multi-agent Reinforcement Learning," *IEEE Trans. Wireless Commun.*, vol. 25, pp. 14 719–14 733, 2026.

[32] Y. Liu, J. Xu, Z. Wang, X. Mu, and L. Hanzo, "Near-field communications: What will be different?" *arXiv preprint arXiv:2303.04003*, 2023.

[33] D.-R. Emenonye, H. S. Dhillon, and R. M. Buehrer, "Ris-aided localization under position and orientation offsets in the near and far field," *arXiv preprint arXiv:2210.03599*, 2022.

[34] J. Wang, J. Xiao, Y. Zou, W. Xie, and Y. Liu, "Wideband beamforming for ris assisted near-field communications," *arXiv preprint arXiv:2401.11141*, 2024.

[35] Y. Chen, X. Guo, G. Zhou, S. Jin, D. W. K. Ng, and Z. Wang, "Unified Far-Field and Near-Field in Holographic MIMO: A Wavenumber-Domain Perspective," *IEEE Commun. Mag.*, vol. 63, pp. 30–36, 2025.

[36] Z. Wang, J. Zhang, W. Yi, H. Xiao, H. Du, D. Niyato, B. Ai, and D. W. K. Ng, "Analytical Framework for Effective Degrees of Freedom in Near-Field XL-MIMO," *IEEE Trans. Wireless Commun.*, vol. 24, pp. 3465–3482, 2025.

[37] W. Chen, Z. Yang, Z. Wei, D. W. K. Ng, and M. Matthaiou, "Ris-aided mimo beamforming: Piece-wise near-field channel model," *arXiv preprint arXiv:2406.14939*, 2024.

[38] C. Ding, J. Zheng, J. Zhang, X. Ge, and D. W. K. Ng, "Resource Allocation for RIS-Assisted Mixed Near- and Far-Field Communication With Directional Antenna," in *in Proc. of the IEEE Wireless Communications and Networking Conference (WCNC)*, 2025.

[39] X. Shao, L. Hu, Y. Sun, X. Li, Y. Zhang, J. Ding, X. Shi, F. Chen, D. W. K. Ng, and R. Schober, "Hybrid Near-Far Field 6D Movable Antenna Design Exploiting Directional Sparsity and Deep Learning," *IEEE Trans. Wireless Commun.*, vol. 25, pp. 3736–3749, 2026.

[40] S. Liu, X. Yu, Z. Gao, J. Xu, D. W. K. Ng, and S. Cui, "Sensing-Enhanced Channel Estimation for Near-Field XL-MIMO Systems," *IEEE J. Sel. Areas Commun.*, vol. 43, pp. 628–643, 2025.

[41] Z. Jin, L. You, D. W. K. Ng, X.-G. Xia, and X. Gao, "Near-Field Channel Estimation for XL-MIMO: A Deep Generative Model Guided by Side Information," *IEEE Trans. Cogn. Commun. Netw.*, vol. 12, pp. 628–643, 2026.

[42] J. Lu, J. Zhang, H. Lei, H. Xiao, B. Ai, and D. W. K. Ng, "Near-field Spatial-domain Channel Extrapolation for XL-MIMO Systems," *IEEE Trans. Wireless Commun.*, vol. 25, pp. 4343–4357, 2026.

[43] L. Qiao, A. Liao, Z. Li, H. Wang, Z. Gao, X. Gao, Y. Su, P. Xiao, L. You, and D. W. K. Ng, "Sensing User's Activity, Channel, and Location with Near-Field Extra-Large-Scale MIMO," *IEEE Trans. Commun.*, vol. 72, no. 2, pp. 890–906, 2024.

[44] W. Hu, Z. He, W. Xu, Y. Huang, D. W. K. Ng, and N. Al-Dhahir, "Energy-Efficient Hybrid Beamfocusing for Near-Field Integrated Sensing and Communication," *IEEE Trans. Signal Process.*, vol. 73, pp. 4011–4026, 2025.

[45] M. Sun, Y. Gong, R. Zhang, Y. Zhao, X. Jing, C. Yuen, and D. W. K. Ng, "Robust Spherical Wavefront Beamforming for Near-Field ISAC with MMSE Optimization: A Distance-Angle Perspective," *IEEE Trans. Commun.*, vol. 74, pp. 6718–6733, 2026.

[46] X. Zhou, F. Ke, C. Wu, X. Y. Zhang, and D. W. K. Ng, "Robust Beamforming for STAR-RIS aided Hybrid-Field ISAC Systems," *IEEE Trans. Commun.*, vol. 74, pp. 5654–5669, 2026.

[47] Y. Wu, D. Xu, D. W. K. Ng, W. Gerstacker, and R. Schober, "Globally Optimal Movable Antenna-Enabled Multiuser Communication: Discrete Antenna Positioning, Power Consumption, and Imperfect CSI," *IEEE Trans. Commun.*, vol. 73, pp. 9903–9923, 2025.

[48] X. Chen, B. Feng, Y. Wu, D. W. K. Ng, and R. Schober, "Two-Timescale Sum-Rate Maximization for Movable Antenna Enhanced Systems," *IEEE Trans. Wireless Commun.*, vol. 25, pp. 3894–3909, 2026.

[49] B. Xu, J. Zhang, S. Chen, Z. Liu, H. Xiao, D. W. K. Ng, and B. Ai, "Multi-Agent Reinforcement Learning for Movable Antenna-aided Cell-Free Massive MIMO Systems," *IEEE J. Sel. Areas Commun.*, 2026.

[50] H. Zhai, J. Zhang, J. Zheng, H. Xiao, H. Jiao, B. Ai, and D. W. K. Ng, "A Joint Optimization Framework for Movable Antenna-Aided Relay Systems," *IEEE Wireless Commun. Lett.*, 2026.

[51] D. Bepari, S. Mondal, A. Bhowal, K. Singh, H. Shin, K.-K. Wong, and D. W. K. Ng, "Fluid Antennas: Pioneering a New Era in Next-Generation Wireless Communications," *IEEE Commun. Surveys Tuts.*, vol. 28, pp. 5596–5631, 2026.

[52] C. Wang, G. Li, H. Zhang, K.-K. Wong, Z. Li, D. W. K. Ng, and C.-B. Chae, "Fluid Antenna System Liberating Multiuser MIMO for ISAC via Deep Reinforcement Learning," *IEEE Trans. Wireless Commun.*, vol. 23, pp. 10 879–10 894, 2024.

[53] X. Zhang, D. Xu, J. Wang, S. Song, D. W. K. Ng, and M. Debbah, "Fluid Antenna Meets RIS: Random Matrix Analysis and Two-Timescale Design for Multi-User Communications," *IEEE J. Sel. Areas Commun.*, vol. 44, pp. 1400–1416, 2026.

[54] S. Mao, C. Yuen, L. Liu, J. Li, Y. Liu, K. Yang, and D. W. K. Ng, "Movable Antenna-Enhanced RIS-Assisted Over-the-Air Computation," *IEEE Trans. Wireless Commun.*, vol. 25, pp. 16 612–16 627, 2026.

[55] B. Xu, J. Zhang, Z. Liu, Z. Wang, B. Ai, and D. W. K. Ng, "Asynchronous Distributed Beamforming for Beyond-Diagonal RIS-aided Movable Antenna Systems," *IEEE Trans. Wireless Commun.*, vol. 25, pp. 4737–4751, 2026.

[56] D. Tyrovolas, S. A. Tegos, P. D. Diamantoulakis, S. Ioannidis, C. K. Liaskos, and G. K. Karagiannidis, "Performance analysis of pinching-antenna systems," *arXiv preprint arXiv:2502.06701*, 2025.

[57] C. Ouyang, Z. Wang, Y. Liu, and Z. Ding, "Capacity characterization of pinching-antenna systems," *arXiv preprint arXiv:2506.14298*, 2025.

[58] Y. Xu, J. Cui, Y. Zhu, Z. Ding, T.-H. Chang, R. Schober, V. W. S. Wong, O. A. Dobre, G. K. Karagiannidis, H. V. Poor, and X. You, "Generalized pinching-antenna systems: A tutorial on principles, design strategies, and future directions," *arXiv preprint arXiv:2510.14166*, 2025.

[59] M. Zeng, J. Wang, O. A. Dobre, Z. Ding, G. K. Karagiannidis, R. Schober, and H. V. Poor, "Resource allocation for pinching-antenna systems: State-of-the-art, key techniques and open issues," *arXiv preprint arXiv:2506.06156*, 2025.

[60] Y. Li, J. Wang, Y. Liu, and Z. Ding, "Pinching-antenna assisted simultaneous wireless information and power transfer," *arXiv preprint arXiv:2505.06240*, 2025.

[61] H. Li, Z. Lyu, Y. Gao, M. Xiao, and H. V. Poor, "Mimo pinching-antenna-aided swipt," *arXiv preprint arXiv:2506.06754*, 2025.

[62] S. Hu, R. Zhao, Y. Liao, D. W. K. Ng, and J. Yuan, "Sum-rate maximization for pinching antenna-assisted NOMA systems with multiple dielectric waveguides," in *Proc. IEEE Global Communications Conference Workshops (GC Wkshps)*, 2025, pp. 411–417.

[63] R. Zhao, S. Hu, D. Mishra, and D. W. K. Ng, "Resource allocation for multi-waveguide pinching antenna-assisted broadcast networks," in *Proc. IEEE Global Commun. Conf. Workshops (GC Wkshps)*, Dec. 2025, pp. 842–848.

[64] ——, "Robust and secure blockage-aware pinching antenna-assisted wireless communication," *IEEE Transactions on Mobile Computing*, 2026.

[65] M. Du, S. Hu, C. Liu, and D. W. K. Ng, "Beamforming for RIS-assisted pinching antenna systems: A deep reinforcement learning approach," in *Proc. IEEE 27th International Workshop on Signal Processing Advances in Wireless Communications (SPAWC)*, 2026.

[66] C. He, Y. Lu, Y. Xu, C.-Y. Chi, B. Ai, and A. Nallanathan, "Ris-assisted downlink pinching-antenna systems: Gnn-enabled optimization approaches," *arXiv preprint arXiv:2511.20305*, 2025.

[67] C. He, Y. Lu, W. Chen, B. Ai, A. Nallanathan, and Z. Ding, "Spectral- and energy-efficient multi-bs multi-ris pinching-antenna systems: A gnn-based approach," *arXiv preprint arXiv:2605.01307*, 2026.